THE ASTROPHYSICAL JOURNAL, 565:280–296, 2002 January 20

SECONDARY ANTIPROTONS AND PROPAGATION OF COSMIC RAYS IN THE GALAXY AND HELIOSPHERE

IGOR V. MOSKALENKO[1,2]
NASA Goddard Space Flight Center, Code 660, Greenbelt, MD 20771; imos@milkyway.gsfc.nasa.gov
ANDREW W. STRONG
Max-Planck-Institut für extraterrestrische Physik, Postfach 1603, D-85740 Garching, Germany; aws@mpe.mpg.de
JONATHAN F. ORMES
NASA Goddard Space Flight Center, Code 600, Greenbelt, MD 20771; jfo@lheapop.gsfc.nasa.gov
AND
MARIUS S. POTGIETER
Unit for Space Physics, Potchefstroom University for CHE, 2520 Potchefstroom, South Africa; fskmsp@puknet.puk.ac.za
Received 2001 June 20; accepted 2001 September 17

ABSTRACT

High-energy collisions of cosmic-ray nuclei with interstellar gas are believed to be the mechanism producing the majority of cosmic-ray antiprotons. Because of the kinematics of the process, they are created with a nonzero momentum; the characteristic spectral shape with a maximum at $\sim$2 GeV and a sharp decrease toward lower energies makes antiprotons a unique probe of models for particle propagation in the Galaxy and modulation in the heliosphere. On the other hand, accurate calculation of the secondary antiproton flux provides a "background" for searches for exotic signals from the annihilation of supersymmetric particles and primordial black hole evaporation. Recently, new data with large statistics on both low- and high-energy antiproton fluxes have become available which allow such tests to be performed. We use our propagation code GALPROP to calculate interstellar cosmic-ray propagation for a variety of models. We show that there is *no* simple model capable of accurately describing the whole variety of data: boron/carbon and sub-iron/iron ratios, spectra of protons, helium, antiprotons, positrons, electrons, and diffuse γ-rays. We find that only a model with a break in the diffusion coefficient plus convection can reproduce measurements of cosmic-ray species, and the reproduction of primaries (p, He) can be further improved by introducing a break in the primary injection spectra. For our best-fit model we make predictions of proton and antiproton fluxes near the Earth for different modulation levels and magnetic polarity using a steady state drift model of propagation in the heliosphere.

Subject headings: cosmic rays — elementary particles — Galaxy: general — ISM: general — nuclear reactions, nucleosynthesis, abundances

1. INTRODUCTION

Most of the cosmic-ray (CR) antiprotons observed near the Earth are secondaries produced in collisions of energetic CR particles with interstellar gas (e.g., Mitchell et al. 1996). Because of the kinematics of this process, the spectrum of antiprotons has a unique shape distinguishing it from other CR species. It peaks at about 2 GeV decreasing sharply toward lower energies. In addition to secondary antiprotons there are possible sources of primary antiprotons; those most often discussed are the dark matter particle annihilation and evaporation of primordial black holes (PBHs).

The nature and properties of the dark matter that constitute a significant fraction of the mass of the universe have puzzled scientists for more than a decade (Trimble 1987; Ashman 1992). Among the favored dark matter candidates are so-called weakly interacting, massive particles (WIMPs), whose existence follows from supersymmetric models (for a review see Jungman, Kamionkowski, & Griest 1996). Such particles, if stable, could have a significant cosmological abundance and be present in our own Galaxy. A pair of stable WIMPs can annihilate into known particles and antiparticles making it possible to infer WIMPs in the Galactic halo by the products of their annihilations. PBHs may have formed in the early universe via initial density fluctuations, phase transitions, or the collapse of cosmic strings (Hawking 1974; Carr 1985; Maki, Mitsui, & Orito 1996). Black holes can emit particles and evaporate as a result of quantum effects. The emission rate is generally too low to be observable, but it increases as the black hole mass decreases. The only observable PBHs are those that have a mass small enough to produce a burst of particles as they evaporate.

In recent years, new data with large statistics on both low- and high-energy antiproton fluxes have become available (Hof et al. 1996; Basini et al. 1999; Orito et al. 2000; Bergström et al. 2000; Maeno et al. 2001; Stochaj et al. 2001; Asaoka et al. 2001b) that allow us to test models of CR propagation and heliospheric modulation. A probe to measure low-energy particles in interstellar space may also become reality in the near future (Mewaldt & Liewer 2001). Additionally, accurate calculation of the secondary antiproton flux provides a "background" for searches for exotic signals such as WIMP annihilation or PBH evaporation.

Despite numerous efforts and overall agreement on the secondary nature of the majority of CR antiprotons, published estimates of the expected flux differ significantly (see, e.g., Fig. 3 in Orito et al. 2000). Calculation of the

[1] NAS/NRC Senior Research Associate.
[2] Also Institute for Nuclear Physics, M. V. Lomonosov Moscow State University, 119 899 Moscow, Russia.

secondary antiproton flux is a complicated task. The major sources of uncertainties are threefold: (1) incomplete knowledge of cross sections for antiproton production, annihilation, and scattering; (2) parameters and models of particle propagation in the Galaxy; and (3) modulation in the heliosphere. While the interstellar antiproton flux is affected only by uncertainties in the cross sections and propagation models, the final comparison with experiment can only be made after correcting for the solar modulation. Besides, the spectra of CR nucleons have been directly measured only inside the heliosphere, while we need to know the spectrum outside, in interstellar space, to compute the antiproton production rate correctly. The basic features of the recent models are summarized in Table 1.

For the antiproton production cross section two options exist: a semiphenomenological fit to the data by Tan & Ng (1983a, 1983b) which has been used for almost two decades because of lack of new data and the Monte Carlo event generator DTUNUC (Ferrari et al. 1996; Roesler, Engel, & Ranft 1998). Both the parameterization and the DTUNUC code describe well the available data on antiproton production in *p-p* collisions. For interactions involving heavier nuclei there are no measurements so far. However, the DTUNUC model provides a reasonable description of hadron-nucleus and nucleus-nucleus interactions, and thus it can be used for estimates of antiproton production in proton-nucleus collisions. Additionally, "tertiary" antiprotons, inelastically scattered secondaries, are the main component at low energies. This component has only been included in the most recent models.

To calculate particle propagation, one must choose between the easy-to-apply but nonphysical "leaky box" model and a variety of diffusion models. The leaky box model reduces the problem to derivation of the path length distribution (which in turn remains the major source of uncertainty as discussed, e.g., by Simon, Molnar, & Roesler 1998). Diffusion models are theoretically more physical but also differ in the degree to which they reflect reality. The ultimate goal is to develop a model which is consistent with many different kinds of data available: measurements of CR species, γ-rays, and synchrotron emission.

Heliospheric modulation is not yet understood in detail. The first and yet popular force field approximation (Gleeson & Axford 1968) does not work at low energies. More sophisticated drift models reflect our still incomplete current knowledge. The main problem here is that the modulation parameters are determined based on the assumed ad hoc interstellar nucleon spectrum. The antiproton/proton ratio, which is often calculated, is even more uncertain at low energies and may vary by an order of magnitude over the solar cycle (Labrador & Mewaldt 1997). It is therefore the antiproton spectrum itself which should be compared with calculations. On the other hand, a reliable calculation of the antiproton spectrum would allow the study of charge sign–dependent effects in the heliosphere. That could, in turn, help to derive the low-energy part of the local interstellar (LIS) spectrum of nucleons and help to establish the heliospheric diffusion coefficients more accurately.

We have developed a numerical method and corresponding computer code GALPROP[3] for the calculation of Galactic CR propagation in three dimensions (Strong & Moskalenko 1998). The code has been shown to reproduce simultaneously observational data of many kinds related to CR origin and propagation (for a review see Strong & Moskalenko 1999; Moskalenko & Strong 2000). The code has been validated on direct measurements of nuclei, antiprotons, electrons, and positrons, as well as astronomical measurements of γ-rays and synchrotron radiation. These data provide many independent constraints on model parameters.

The code is sufficiently general that new physical effects can be introduced as required. The basic spatial propagation mechanisms are diffusion and convection, while in momentum space energy loss and diffusive reacceleration are treated. Fragmentation, secondary particle production, and energy losses are computed using realistic distributions for the interstellar gas and radiation fields. Recently, the code has been entirely rewritten in C++ with many new features added (Strong & Moskalenko 2001).

In this paper we use the GALPROP code for accurate calculation of production and propagation of secondary antiprotons and positrons. We explore the dependence of the antiproton and positron fluxes on the nucleon injection spectrum and propagation parameters. The antiproton production cross section is calculated using the *p-p* production cross section (Tan & Ng 1983b) and DTUNUC nuclear

[3] Our model including software and data sets is available at http://www.gamma.mpe-garching.mpg.de/~aws/aws.html.

TABLE 1

SUMMARY OF RECENT CR ANTIPROTON CALCULATIONS

Model	Antiproton Production	Ambient CR Spectrum	Propagation Model	Reacceleration/ Convection	Modulation in Heliosphere	Tertiary Antiprotons
Bergström et al. (1999)...	Tan & Ng	Scaled LIS	Simplified diffusion	No/Yes	Force field	Yes
Bieber et al. (1999)	DTUNUC event generator	LIS, in the whole Galaxy	Leaky box	No/No	Steady state drift model[a]	Yes
Bottino et al. (1998).....	Tan & Ng	LIS, in the whole Galaxy	Two-zone diffusion	No/No	Force field	No
Donato et al. (2001).....	Tan & Ng, DTUNUC	LIS, in the whole Galaxy	Two-zone diffusion	Yes/Yes	Force field	Yes
Simon et al. (1998)	DTUNUC event generator	LIS, in the whole Galaxy	Leaky box	No/No	Force field	No
Present work	*p-p*: Tan & Ng; *p-A*: DTUNUC	Propagated	Three-dimensional spatial grid, realistic diffusion	Yes/Yes	Steady state drift model	Yes

[a] Parameters are fixed from the assumed local interstellar (LIS) proton spectrum.

factors from Simon et al. (1998) to calculate $\bar{p}$ production in p-A collisions or the p-p production cross section scaled appropriately with beam/target atomic numbers. Inelastic scattering to produce "tertiary" antiprotons and "secondary" protons is taken into account. The calculated proton and antiproton LIS and $\bar{p}/p$ ratio are modulated using the steady state drift model. Our preliminary results have been reported in Moskalenko et al. (2001b).

2. BASIC FEATURES OF THE GALPROP MODELS

The cylindrically symmetric GALPROP models have been described in detail elsewhere (Strong & Moskalenko 1998); here we summarize their basic features.

The models are three-dimensional with cylindrical symmetry in the Galaxy, and the basic coordinates are (R, z, p), where R is Galactocentric radius, z is the distance from the Galactic plane, and p is the total particle momentum. In the models the propagation region is bounded by $R = R_h$, $z = \pm z_h$ beyond which free escape is assumed.

The propagation equation we use for all CR species is written in the form

$$\frac{\partial \psi}{\partial t} = q(\mathbf{r}, p) + \nabla \cdot (D_{xx} \nabla \psi - \mathbf{V} \psi) + \frac{\partial}{\partial p} p^2 D_{pp} \frac{\partial}{\partial p} \frac{1}{p^2} \psi - \frac{\partial}{\partial p} \left[\dot{p} \psi - \frac{p}{3} (\nabla \cdot \mathbf{V}) \psi \right] - \frac{1}{\tau_f} \psi - \frac{1}{\tau_r} \psi , \quad (1)$$

where $\psi = \psi(\mathbf{r}, p, t)$ is the density per unit of total particle momentum, $\psi(p)dp = 4\pi p^2 f(\mathbf{p})$ in terms of phase-space density $f(\mathbf{p})$, $q(\mathbf{r}, p)$ is the source term, D_{xx} is the spatial diffusion coefficient, $\mathbf{V}$ is the convection velocity, reacceleration is described as diffusion in momentum space and is determined by the coefficient D_{pp}, $\dot{p} \equiv dp/dt$ is the momentum loss rate, τ_f is the timescale for fragmentation, and τ_r is the timescale for radioactive decay. The numerical solution of the transport equation is based on a Crank-Nicholson (Press et al. 1992) implicit second-order scheme. The three spatial boundary conditions $\psi(R_h, z, p) = \psi(R, \pm z_h, p) = 0$ are imposed on each iteration, where we take $R_h = 30$ kpc.

For a given z_h the diffusion coefficient as a function of momentum and the reacceleration or convection parameters is determined by boron-to-carbon (B/C) ratio data. The spatial diffusion coefficient is taken as $D_{xx} = \beta D_0 (\rho/\rho_0)^{\delta}$ if necessary with a break ($\delta = \delta_1$ below rigidity ρ_0, $\delta = \delta_2$ above rigidity ρ_0). The injection spectrum of nucleons is assumed to be a power law in momentum, $dq(p)/dp \propto p^{-\gamma}$ for the injected particle density.

Reacceleration provides a mechanism to reproduce the B/C ratio without an ad hoc form for the diffusion coefficient. Our reacceleration treatment assumes a Kolmogorov spectrum with $\delta = \frac{1}{3}$ or a value close to this. For the case of reacceleration the momentum space diffusion coefficient D_{pp} is related to the spatial coefficient D_{xx} (Berezinskii et al. 1990; Seo & Ptuskin 1994) via the Alfvén speed v_A.

The convection velocity (in z-direction only) $V(z)$ is assumed to increase linearly with distance from the plane ($dV/dz > 0$ for all z). This implies a constant adiabatic energy loss; the possibility of adiabatic energy gain ($dV/dz < 0$) is not considered. The linear form for $V(z)$ is consistent with CR-driven MHD wind models (e.g., Zirakashvili et al. 1996). The velocity at $z = 0$ is a model parameter, but we consider here only $V(0) = 0$. [$V(0) = 0$ is physically plausible: it is required to avoid a discontinuity, since by symmetry a nonzero velocity would have to change sign at $z = 0$.]

The interstellar hydrogen distribution uses H I and CO surveys and information on the ionized component; the helium fraction of the gas is taken as 0.11 by number. The H_2 and H I gas number densities in the Galactic plane are defined in the form of tables, which are interpolated linearly. The extension of the gas distribution to an arbitrary height above the plane is made using analytical approximations. The distributions of $2 \times H_2$, H I, and H II are plotted on Figure 1 for $z = 0$, 0.1, and 0.2 kpc. The code uses the densities averaged over the z-grid using a 0.01 kpc step. More details about the gas distribution model are given in Appendix A.

The distribution of CR sources is chosen to reproduce the CR distribution determined by analysis of EGRET γ-ray data (Strong & Mattox 1996) and was described in Strong & Moskalenko (1998).

Energy losses for nucleons by ionization and Coulomb interactions are included, and for electrons by ionization, Coulomb interactions, bremsstrahlung, inverse Compton (IC), and synchrotron.

Positrons and electrons (including secondary electrons) are propagated in the same model. Positron production is computed as described in Moskalenko & Strong (1998); that paper includes a critical reevaluation of the secondary $\pi^{\pm}$- and $K^{\pm}$-meson decay calculations.

Gas-related γ-ray intensities are computed from the emissivities as a function of (R, z, E_γ) using the column densities of H I and H_2. The interstellar radiation field (ISRF), used for calculation of the IC emission and electron energy

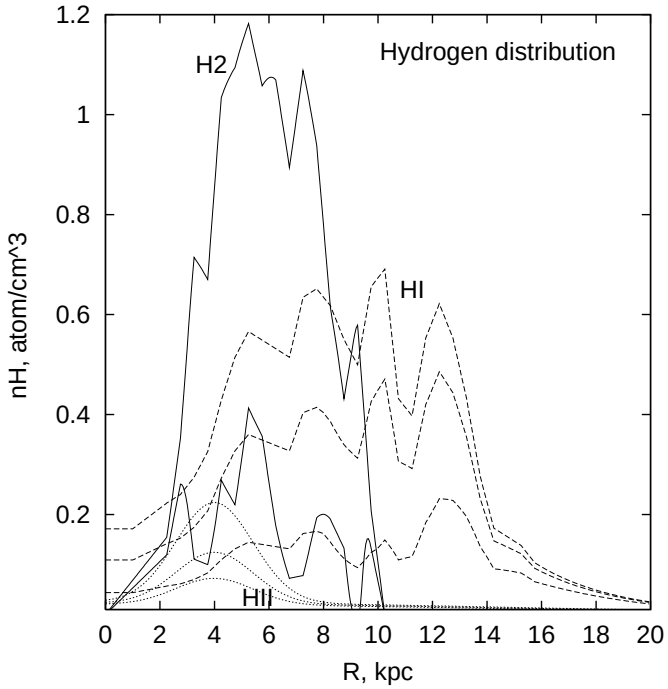

FIG. 1.—Number density distributions of $2 \times H_2$ (*solid lines*), H I (*dashed lines*), and H II (*dotted lines*) in the Galaxy. Shown are the plots for $z = 0$, 0.1, and 0.2 kpc (decreasing density). Number density of H_2 at $z = 0.2$ kpc from the plane is very low and is not shown in the plot.

losses, is calculated based on stellar population models and *COBE* results, plus the cosmic microwave background.

An overview of our previous analyses is presented in Strong & Moskalenko (1999) and Moskalenko & Strong (2000) and full results for protons, helium, positrons, and electrons in Moskalenko & Strong (1998) and Strong, Moskalenko, & Reimer (2000). The evaluations of the B/C and ^{10}Be/^{9}Be ratios, diffusion/convection and reacceleration models, and full details of the numerical method are given in Strong & Moskalenko (1998). Antiprotons have been previously discussed in the context of the "hard interstellar nucleon spectrum" hypothesis in Moskalenko, Strong, & Reimer (1998) and Strong et al. (2000). Our results for diffuse continuum γ-rays, synchrotron radiation, and a new evaluation of the ISRF are described in Strong et al. (2000).

2.1. *New Developments*

The experience gained from the original FORTRAN-90 code allowed us to design a new version of the model, entirely rewritten in C++, that is much more flexible. It allows essential optimizations in comparison to the older model and a full three-dimensional spatial grid. It is now possible to explicitly solve the full nuclear reaction network on a spatially resolved grid. The code can thus serve as a complete substitute for the conventional "leaky box" or "weighted-slab" propagation models usually employed, giving many advantages such as the correct treatment of radioactive nuclei, realistic gas and source distributions, etc. It also allows stochastic supernova remnant (SNR) sources to be included. It still contains an option to switch to the fast-running cylindrically symmetrical model which is sufficient for many applications such as the present one.

In the new version, we have updated the cross section code to include the latest measurements and energy-dependent fitting functions. The nuclear reaction network is built using the Nuclear Data Sheets. The isotopic cross section database consists of more than 2000 points collected from sources published in 1969–1999. This includes a critical reevaluation of some data and cross-checks. The isotopic cross sections are calculated using the author's fits to major beryllium and boron production cross sections p + C, N, O $\rightarrow$ Be, B. Other cross sections are calculated using Webber, Kish, & Schrier (1990)[4] and/or Silberberg, Tsao, & Barghouty (1998)[5] phenomenological approximations renormalized to the data where they exist. The cross sections on the He target are calculated using a parameterization by Ferrando et al. (1988).

The reaction network is solved starting at the heaviest nuclei (i.e., ^{64}Ni). The propagation equation is solved, computing all the resulting secondary source functions, and then proceeds to the nuclei with $A - 1$. The procedure is repeated down to $A = 1$. In this way all secondary, tertiary, etc., reactions are automatically accounted for. This includes secondary protons, inelastically scattered primaries; their energy distribution after scattering is assumed to be the same as for antiprotons (eq. [2]). To be completely accurate for all isotopes, e.g., for some rare cases of $\beta^{\pm}$-decay, the whole loop is repeated twice. Our preliminary results for all CR species $Z \leq 28$ are given in Strong & Moskalenko (2001).

For the calculation reported here, we use a cylindrically symmetrical Galactic geometry.

2.2. *Antiproton Cross Sections*

We calculate $\bar{p}$ production and propagation using the basic formalism described in Moskalenko et al. (1998). Antiproton production in p-p collisions has been calculated using the parameterization of the invariant $\bar{p}$ production cross section given by Tan & Ng (1983b). This parameterization fits available data quite well. It gives an antiproton multiplicity slightly higher than the DTUNUC code just above the threshold and agrees with DTUNUC results at higher energies (Simon et al. 1998).

For the cross sections $\sigma_{pp}^{\rm inel}$ and $\sigma_{pA}^{\rm inel}$ we adapted parameterizations by Tan & Ng (1983a), Groom et al. (2000), and Letaw, Silberberg, & Tsao (1983). At low energies the total $\bar{p}$-p inelastic cross section has been calculated using a fit from Tan & Ng (1983a). At high energies it is calculated as the difference between total $\bar{p}$-p and p-p cross sections which are parameterized using Regge theory (Groom et al. 2000). The $\bar{p}$ absorption cross section on an arbitrary nuclear target has been scaled by $A^{2/3}$ using the measured $\bar{p}$ − C, Al, Cu cross sections (Moiseev & Ormes 1997).

To this we have added $\bar{p}$ annihilation and treated inelastically scattered antiprotons as a separate "tertiary" component. The energy distribution after scattering is assumed to be (Tan & Ng 1983a)

$$\frac{dN(E_{\bar{p}}, E'_{\bar{p}})}{dE_{\bar{p}}} = \frac{1}{T'_{\bar{p}}}\,, \tag{2}$$

where $E'_{\bar{p}}$ and $E_{\bar{p}}$ are the total $\bar{p}$ energy before and after scattering, respectively, and $T'_{\bar{p}}$ is the $\bar{p}$ kinetic energy before scattering.

The $\bar{p}$ production by nuclei with $Z \geq 2$ is calculated using effective nuclear factors by Simon et al. (1998) and scaling factors similar to Gaisser & Schaefer (1992).

In the first method we use the effective factor obtained from simulations of the $\bar{p}$ production with the Monte Carlo model DTUNUC, which appear to be more accurate than simple scaling. The use of this factor is consistent since the proton spectrum adapted in Simon et al. (1998) is close to our propagated spectrum above the $\bar{p}$ production threshold. For convenience, we made a fit to the ratio of the total $\bar{p}$ yield to the $\bar{p}$ yield from the p-p reaction (col. [3]/col. [2] ratio as given in Table 2 in Simon et al. 1998):

$$\frac{\sigma_{\Sigma}}{\sigma_{pp}} = 0.12\left(\frac{T_{\bar{p}}}{\rm GeV}\right)^{-1.67} + 1.78\,, \tag{3}$$

where $T_{\bar{p}}$ is the kinetic $\bar{p}$ energy.

In the second method the cross section for $\bar{p}$ production in proton-nucleus and nucleus-nucleus interactions has been obtained by scaling the p-p invariant cross section with a factor (Gaisser & Schaefer 1992)

$$F_{it\rightarrow\bar{p}X} = \frac{1.2(A_i\,\sigma_{pt}^{\rm inel} + A_t\,\sigma_{pi}^{\rm inel})}{2\sigma_{pp}^{\rm inel}}\,, \tag{4}$$

where $A_{i,t}$ are the atomic numbers of the incident and target nuclei, σ_{pt} and σ_{pi} are the $pA_{i,t}$ cross sections, and a factor 1.2 is put for consistency with Simon et al. (1998) calcu-

[4] Code WNEWTR.FOR, Version 1993, as posted at http://spdsch.phys.lsu.edu/SPDSCH_Pages/Software_Pages/Cross_Section_Calcs/WebberKishSchrier.html (some minor changes have been made to make it compatible with GALPROP).

[5] Code YIELDX_011000.FOR, Version 2000, as posted at http://spdsch.phys.lsu.edu/SPDSCH_Pages/Software_Pages/Cross_Section_Calcs/SilberburgTsao.html (some minor changes have been made to make it compatible with GALPROP).

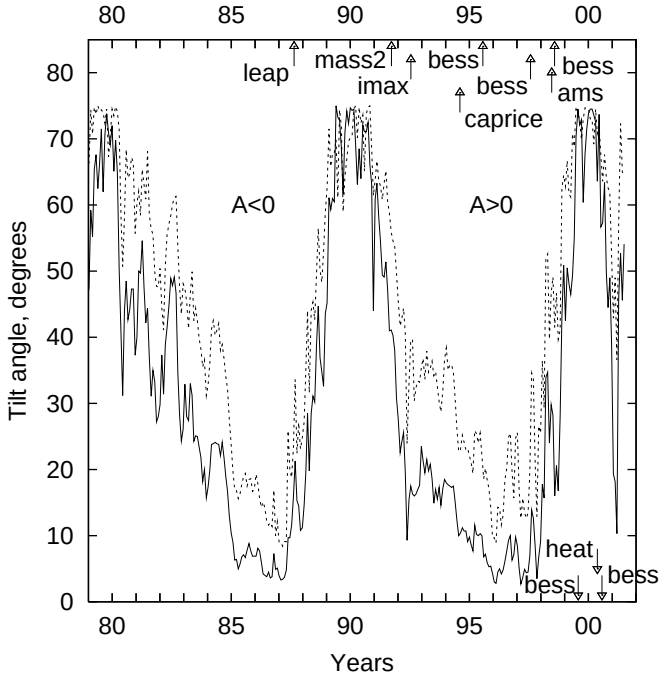

FIG. 2.—Heliospheric current sheet tilt angles for two Hoeksema models (e.g., Hoeksema 1992; Zhao & Hoeksema 1995), the classic "L model" (*dashed line*) and a newer "R model" (*solid line*).

lations. Production of low-energy antiprotons in p-α and α-α reactions is increased over that for simple scaling. In order to account for this effect, we put $\tilde{E}_{\bar{p}} = E_{\bar{p}} + 0.06$ GeV instead of $E_{\bar{p}}$ when calculating the source spectra.

Detailed results published by Simon et al. (1998; their Figs. 2, 4, and 7) allow us to test the approximation given by equation (4) and show its equivalence to DTUNUC calculations and to equation (3). For these tests we used interstellar proton and helium spectra as published by Menn et al. (2000); these spectra were used by Simon et al. (1998). The main discrepancy is $\sim$15%–20% underproduction of antiprotons in p-p collisions in the range $T_{\bar{p}} = 5$–30 GeV compared to Simon et al. (1998) calculations (their Fig. 7), but this does not influence production and propagation of antiprotons at lower energies. At energies below $\sim$5 GeV the factors given by equations (3) and (4) are virtually equivalent. We further use equation (3) in our calculations.

The $\bar{p}$-p elastic scattering is not included. At sufficiently high energies it is dominated by the forward peak with small energy transfer while at low energies the inelastic cross section (mostly annihilation) accounts for about 70% of the total cross section (Eisenhandler et al. 1976; Brückner et al. 1986).

As we will see, the accuracy of antiproton cross sections is now a limiting factor; we therefore summarize the current status in Appendix B.

3. SOLAR MODULATION

Thanks to the *Ulysses* mission significant progress has been made in our understanding of the major mechanisms driving the modulation of CRs in the heliosphere. The principal factors in modulation modeling are the heliospheric magnetic field (HMF), the solar wind speed, the tilt of the heliospheric current sheet (HCS), and the diffusion tensor. Here we give a short description of the model used in this paper for modulation of Galactic protons and antiprotons. More detail on the characteristics of heliospheric modulation and modulation models can be found elsewhere (e.g., Potgieter 1997; Burger, Potgieter, & Heber 2000 and references therein).

Modulation models are based on the numerical solution of the CR transport equation (Parker 1965):

$$\frac{\partial f(\boldsymbol{r}, \rho, t)}{\partial t} = -(\boldsymbol{V} + \langle \boldsymbol{v}_D \rangle) \cdot \nabla f + \nabla \cdot (\boldsymbol{K}_S \cdot \nabla f) + \frac{1}{3} (\nabla \cdot \boldsymbol{V}) \frac{\partial f}{\partial \ln \rho}, \quad (5)$$

where $f(\boldsymbol{r}, \rho, t)$ is the CR distribution function, $\boldsymbol{r}$ is the position, ρ is the rigidity, and t is time. Terms on the right-hand side represent convection, gradient and curvature drifts, diffusion, and adiabatic energy losses, respectively, with $\boldsymbol{V}$ the solar wind velocity. The symmetric part of the tensor $\boldsymbol{K}_S$ consists of diffusion coefficients parallel ($K_{\parallel}$) and perpendicular ($K_{\perp\theta}$ and $K_{\perp r}$) to the average HMF. The antisymmetric element K_A describes gradient and curvature drifts in the large-scale HMF where the pitch angle averaged guiding center drift velocity for a near isotropic CR distribution is given by $\langle \boldsymbol{v}_D \rangle = \nabla \times K_A \boldsymbol{e}_B$, with $\boldsymbol{e}_B = \boldsymbol{B}/B$ and B the magnitude of the background magnetic field. The effective radial diffusion coefficient is given by $K_{rr} = K_{\parallel} \cos^2 \psi + K_{\perp r} \sin^2 \psi$, with ψ the angle between the radial direction and the averaged magnetic field direction. We enhanced perpendicular diffusion in the polar direction by assuming $K_{\perp\theta} > K_{\perp r}$ in the heliospheric polar regions (see also Potgieter 2000).

Drift models predict a clear charge sign dependence for the heliospheric modulation of positively charged particles, e.g., CR protons and positrons, and negatively charged particles, e.g., electrons and antiprotons. This is due to the different large-scale gradient, curvature and current sheet drifts that charged particles experience in the HMF. For example, antiprotons will drift inward primarily through the polar regions of the heliosphere during $A < 0$ polarity cycles, when the HMF is directed toward the Sun in the northern hemisphere. Protons, on the other hand, will then drift inward primarily through the equatorial regions of the heliosphere, encountering the wavy heliospheric current sheet in the process. During the $A > 0$ polarity cycles, the drift directions for the two species reverse, so that a clear 22 yr cycle is caused (e.g., Burger & Potgieter 1999).

We use a steady state two-dimensional model that simulates the effect of a wavy current sheet (Hattingh & Burger 1995) by using an averaged drift field with only r- and θ-components for the three-dimensional drift pattern in the region swept out by the wavy current sheet. The solar wind speed is 400 km s^{-1} in the equatorial plane and increases to 800 km s^{-1} in the polar regions (for details see Burger et al. 2000). A modified HMF is used (Jokipii & Kóta 1989). The outer boundary is assumed to be at 120 AU.

The diffusion tensor is described in detail by Burger et al. (2000), who used the same models for turbulence (Zank, Matthaeus, & Smith 1996) but have adapted the coefficients to reflect some of the results from the numerical simulations (Giacalone & Jokipii 1999; Giacalone, Jokipii, & Kóta 1999).

The model used here gives latitudinal gradients in excellent agreement with *Ulysses* observations, for both its value and its rigidity dependence (Burger et al. 2000). The model

also gives realistic radial dependence for CR protons during consecutive solar minima, with the radial gradients distinctly smaller in the $A > 0$ than in the $A < 0$ cycles. Detailed fits to *Pioneer* and *Voyager* observations require that different diffusion coefficients must be used for consecutive solar minimum periods (Potgieter 2000).

The maximum extent of the HCS (tilt angle) has been used in modulation models as a proxy for solar activity since the 1970s, when it was realized that drifts were important. Figure 2 shows the tilt angle,[6] which is used as input in our modulation calculations, for two of Hoeksema's models (classic "L model" and a newer "R model") versus time. The upper and lower curves represent his old and new model, respectively (e.g., Hoeksema 1992; Zhao & Hoeksema 1995). The difference between the models illustrates the error in the tilt angles one has to consider when used in any modulation modeling.

4. ANTIPROTON MEASUREMENTS

Golden et al. (1979) and independently Bogomolov et al. (1979) reported the first measurements of CR antiprotons. Both experiments employed a superconducting magnet for measuring momentum and a gas Cerenkov detector to separate the background of other negatively charged particles from antiprotons. These were the first attempts to measure the flux near the 2 GeV peak expected (Gaisser & Levy 1974) in the differential spectrum of secondary antiprotons in CRs. The flux found was a factor of ~ 3 above that expected and caused a stir at the time. However, the statistics and systematic errors in both the measurement and the theory of that time were such that the excess was significant at about the 3 σ level. With the clarity of hindsight (see below), the Golden et al. (1979) and Bogomolov et al. (1979) measurements were probably plagued by a background of negatively charged particles that went undetected by the Cerenkov detector.

An annihilation technique (Buffington, Schindler, & Pennypacker 1981) was used to make the first alleged measurement of lower energy antiprotons (less than 1 GeV). This technique was designed to stop the antiprotons in a visualization device. Antiprotons were identified by limiting their intrinsic kinetic energy (less than 500 MeV) and finding their rest energy (~ 2 GeV) from the number of annihilation prongs and large energy release. We now know that this experiment must also have been plagued by a high background of interacting particles because the flux of ~ 200 MeV antiprotons found exceeds that of more recent measurements by more than an order of magnitude.

However, these papers stimulated the realization that antiprotons could be produced by exotic processes such as the annihilation of PBHs or dark matter in the Galactic halo (e.g., Carr 1985; Maki et al. 1996; Szabelski, Wdowczyk, & Wolfendale 1980; Kiraly et al. 1981; Silk & Srednicki 1984; Rudaz & Stecker 1988; Ellis et al. 1988; Stecker & Tylka 1989; Jungman & Kamionkowski 1994; Chardonnet et al. 1996).

During the past 5 yr, the BESS (Balloon-borne Experiments with a Superconducting Solenoid) Collaboration (Yamamoto et al. 1993) has made a set of accurate new measurements that motivated this attempt to make a more accurate model calculation. This impressive payload now has data that extend from about 200 MeV (at the top of the atmosphere) to 4 GeV. Importantly, this covers the energy range of the expected peak in the antiproton distribution at 2 GeV where the flux is highest. The first reported mass-resolved measurements (Ahlen et al. 1988; Salamon et al. 1990; Yoshimura et al. 1995; Mitchell et al. 1996) of antiprotons were made at lower energies where determining both the momentum per unit charge (rigidity) and velocity was easier. As can be seen from equation (6), both are needed to determine the mass:

$$m^2 \propto \rho^2(\beta^{-2} - 1) , \tag{6}$$

where $\beta = v/c$, the velocity, and η, the curvature, are the measured parameters. Rigidity, $\rho = 1/\eta$, is inversely proportional to the curvature. Uncertainties are given by

$$\frac{(\Delta m)^2}{m^2} = \frac{(\Delta \rho)^2}{\rho^2} + \frac{(\Delta \beta)^2}{\beta^2(1 - \beta^2)^2} . \tag{7}$$

The statistical precision in these first measurements was poor (Yoshimura 2001).

In BESS the charge sign and rigidity are determined by track measuring drift chambers located in the uniform magnetic field inside the bore of their superconducting magnet. Extending to higher energy has required the use of not only the most precise time of flight measurement but also the addition of aerogel Cerenkov detectors for measuring velocity. The BESS team, through a series of annual balloon campaigns in Lynn Lake, Manitoba, Canada, has continuously improved the time resolution, and in 1997 they added an aerogel counter, extending the energy coverage beyond 2 GeV. In addition, the data handling capacity has continuously improved to decrease dead time and increase precision.

In this paper we use mainly BESS data collected in 1995 and 1997 (Orito et al. 2000). However, in one plot (§ 6), we have combined the data from those BESS flights with their 1998 data (Maeno et al. 2001) after correcting it for increased solar modulation level. The flights in 1995 and 1997 took place near solar minimum conditions, while the 1998 flight was just after solar modulation minimum (Fig. 2). We compare our predictions for different heliospheric modulation levels with data from BESS flights in 1995–1997, 1998, 1999, and 2000 (Orito et al. 2000; Maeno et al. 2001; Asaoka et al. 2001b) in the figures discussed in § 6. The BESS flight in 2000 provides the first accurate measurement of the $\bar{p}/p$ ratio for the negative polarity solar cycle.

The statistical precision with which the flux at 2 GeV is known is now better than 10% (1 σ). The data are now good enough to detect solar modulation effects at this energy at about the same magnitude. The BESS group has carried out an extensive calibration of their instrument to check for ways to reduce sources of systematic error. They report a systematic uncertainty in the antiproton flux measurements to be about 5% (Asaoka et al. 2001a).

Data at energies above 4 GeV on the steeply falling part of the antiproton spectrum are more difficult to obtain. We have used the results reported by the MASS group (Hof et al. 1996; Basini et al. 1999) from a flight in 1991 based on the original Golden et al. (1979) payload but with an improved gas Cerenkov detector; we have used their most recent analysis (Stochaj et al. 2001). These data have error bars that extend up and down by a factor of ~ 2. We can say that they are consistent with antiprotons being of secondary origin but are not precise enough to place constraints on the model presented here.

[6] See http://quake.stanford.edu/~wso.

TABLE 2

PARAMETERS OF THE LIS PROTON SPECTRUM[a] AS DERIVED IN THE PRESENT PAPER

Instrument	Fitting Interval E_{kin} (GeV)	Normalization $(m^2\ s\ sr\ GeV)^{-1}$	Power-Law Index	Modulation Potential (MV)	Fit Quality, χ^2_n	Flight Date	Data Reference
LEAP.....	20–100	...	2.69 ± 0.04	550	0.80	1987 Aug 21	1
MASS2	20–100	$(1.93 \pm 0.15) \times 10^4$	2.82 ± 0.03	1200	0.53	1991 Sep 23	2
IMAX	20–200	$(1.08 \pm 0.15) \times 10^4$	2.66 ± 0.04	750	0.26	1992 Jul 16–17	3
CAPRICE.....	20–200	$(1.55 \pm 0.19) \times 10^4$	2.80 ± 0.03	600	2.54	1994 Aug 8–9	4
AMS	20–200	$(1.82 \pm 0.21) \times 10^4$	2.79 ± 0.03	550	0.13	1998 Jun	5
BESS	20–120	$(1.61 \pm 0.13) \times 10^4$	2.75 ± 0.03	550	0.05	1998 Jul 29–30	6
Weighted average...		$(1.58 \pm 0.08) \times 10^4$	2.76 ± 0.01				

[a] Assuming power law in kinetic energy LIS spectrum.

REFERENCES.—(1) Seo et al. 1991. (2) Belotti et al. 1999. (3) Menn et al. 2000. (4) Boezio et al. 1999. (5) Alcaraz et al. 2000a. (6) Sanuki et al. 2000.

5. NEW CALCULATIONS

5.1. *Local Proton and Helium Spectra*

Secondary antiprotons are produced in collisions of energetic protons and helium nuclei with interstellar gas, so the interstellar spectra of these nuclei are fundamental to calculating antiproton spectra expected at Earth. A major problem in determination of the LIS CR spectrum is the effect of heliospheric modulation that has been discussed in detail in § 3. Inverting equation (5) is *not* well defined, making the accurate derivation of the LIS spectrum a complicated task. However, at energies above the antiproton production threshold, at 10–30 GeV nucleon^{-1}, the heliospheric modulation is weak. We thus try to get an approximate LIS spectrum using the force field approximation (Gleeson & Axford 1968). The appropriate modulation potential (Φ) has been chosen using CLIMAX neutron monitor data (Badhwar & O'Neill 1996).

Spectra given in the literature are quoted in different ways, sometimes as power laws in kinetic energy, sometimes rigidity or total energy. In addition, different measurements have different systematic uncertainties in flux. In order to best determine the asymptotic slope of the locally observed spectrum, we have summarized all recent measurements and fitted them assuming an LIS spectrum which is a power law in kinetic energy. (We note that fitting to a power law in rigidity yields the spectrum which is too steep to agree with high-energy data by Sokol and JACEE.)

To get an idea of which part of the nucleon spectrum contributes most to antiproton production, we have made runs in which we cut the nucleon spectrum at different energies. Our analysis shows that ~97% of all antiprotons below 6 GeV are produced by nucleons below ~200 GeV nucleon^{-1}. The nucleons at $\leq$20 GeV nucleon^{-1} yield about $\frac{1}{3}$ of all antiprotons $\leq$1 GeV, nucleons of $\leq$50 GeV nucleon^{-1} yield about 80% of all antiprotons $\leq$2 GeV, and 90% of antiprotons $\leq$4 GeV are produced by nucleons of $\leq$100 GeV nucleon^{-1}. Therefore, the spectra at moderate energies, up to ~200 GeV nucleon^{-1}, are of most importance.

Tables 2 and 3 show our fits to recent measurements of CR protons and helium. (The power law in kinetic energy has been modulated with appropriate modulation potential and then fitted to the data.) From the parameters fitted to each individual set of measurements we calculate the weighted averages. The reduced χ^2_n (χ^2 per the degree of freedom) shows the quality of the fits.

The fitted parameters are not unique since the modulation potential is not well determined and on account of the systematic and statistical errors. We therefore use also representative high-energy data, above ~100 GeV nucleon^{-1}, where the modulation has no effect, for a cross-check. In particular, our composite proton spectrum, $1.60 \times 10^4 E_{kin}^{-2.75}$ m^{-2} s^{-1} sr^{-1} GeV^{-1}, passes through Sokol (Ivanenko et al. 1993) and JACEE data points (Asakimori et al. 1998). The index agrees well with that determined by Ryan, Ormes, & Balasubrahmanyan (1972), 2.75 ± 0.03, and HEGRA below the knee (HEGRA Collaboration 2000), $2.72^{+0.02}_{-0.03} \pm 0.07$. The derived LIS proton spectrum thus agrees very well with all the data in the range ~10–10^5 GeV.

Our calculation of the nucleon spectrum is based on the solution of the diffusion equation (1), which gives the spectrum in every cell of the spatial grid. Shock acceleration

TABLE 3

PARAMETERS OF THE LIS HELIUM SPECTRUM[a] AS DERIVED IN THE PRESENT PAPER

Instrument	Fitting Interval E_{kin} (GeV nucleon^{-1})	Normalization $(m^2\ s\ sr\ GeV\ nucleon^{-1})^{-1}$	Power-Law Index	Modulation Potential (MV)	Fit Quality, χ^2_n	Flight Date	Data Reference
LEAP.....	10–100	...	2.69 ± 0.09	550	...	1987 Aug 21	1
MASS2	10–50	686 ± 130	2.79 ± 0.07	1200	0.44	1991 Sep 23	2
IMAX	10–125	600 ± 120	2.70 ± 0.07	750	0.69	1992 Jul 16–17	3
CAPRICE.....	10–100	590 ± 124	2.73 ± 0.07	600	0.66	1994 Aug 8–9	4
AMS	10–100	653 ± 56	2.72 ± 0.03	550	0.39	1998 Jun	5
BESS	10–50	640 ± 139	2.67 ± 0.07	550	0.14	1998 Jul 29–30	6
Weighted average...		641 ± 53	2.72 ± 0.01				

[a] Assuming power law in kinetic energy per nucleon LIS spectrum.

REFERENCES.—(1) Seo et al. 1991. (2) Belotti et al. 1999. (3) Menn et al. 2000. (4) Boezio et al. 1999. (5) Alcaraz et al. 2000b. (6) Sanuki et al. 2000.

models predict that the injection CR spectrum can be approximated by a power law in rigidity which may steepen at low energies (e.g., Ellison, Slane, & Gaensler 2001). Hence, we adopt a power law in rigidity, if necessary with a break, for the injection spectrum. The local measurements are conventionally used for comparison and normalization of the propagated spectrum. While there are some indications that the LIS nucleon spectrum may be not representative (Strong et al. 2000), at high energies where the diffusion is fast and energy losses become small it should be close to that observed near the Earth. This is also indicated by studies of Galactic diffuse emission, antiprotons, and positrons (Hunter et al. 1997; Moskalenko et al. 1998; Strong et al. 2000). While our propagation calculations yield LIS spectra which cannot be described by a single power law, the estimates together with data will serve as useful guidelines.

The propagated helium spectrum with an appropriate normalization matches after modulation the data better than the averaged LIS spectrum from Table 3. The latter is somewhat too low when compared with high-energy data by Sokol and JACEE.

5.2. *Propagation Models and Parameters*

To investigate the range of interstellar spectra and propagation parameters, we have run a large number of models. Here we consider five cases (see Table 4), which differ in Galactic propagation. The diffusive reacceleration (DR) model has been chosen since it has been very successful in the description of the propagation of CR nuclei; it reproduces the sharp peak in the secondary to primary nuclei ratios in a physically understandable way without breaks in the diffusion coefficient and/or the injection spectrum. We consider also a diffusive reacceleration model with break in the injection spectrum (DRB) in order to match the LIS proton and He spectra. The minimal reacceleration plus convection (MRC) model uses reduced reacceleration, and in addition some convection is invoked to reproduce the B/C ratio. We compute also a plain diffusion (PD) model for reference, although it does not fit B/C. In the fifth model we use diffusion and convection (DC) with breaks in the diffusion coefficient and the injection index in order to construct a model capable of describing all the CR (particle) data simultaneously.

In all models, the injection spectrum was chosen to reproduce the local CR measurements (see § 5.1). The source abundances of all isotopes $Z \leq 28$ are given in Strong & Moskalenko (2001). The propagation parameters have been fixed using the B/C ratio. Because of the cross section fits to the main Be and B production channels and renormalization to the data where they exist, the propagation parameters show only weak dependence ($\sim 10\%$ change in the diffusion coefficient) on the cross section parameterization (Silberberg et al. 1998; Webber et al. 1990). We thus use Webber et al. (1990) cross section code in our calculations.

The halo size has been set to $z_h = 4$ kpc, which is within the range $z_h = 3$–7 kpc derived using the GALRPOP code and the combined measurements of radioactive isotope abundances, ^{10}Be, ^{26}Al, ^{36}Cl, and ^{54}Mn (Strong & Moskalenko 2001). This is also in agreement with our newer estimate $z_h = 4$–6 kpc (Moskalenko, Mashnik, & Strong 2001a). Note that the exact value of z_h is unimportant for antiproton calculations provided that the propagation parameters are tuned to match the B/C ratio.

Our results are plotted in Figures 3–7. The upper curve is always the LIS spectrum, except in the B/C ratio plot (Fig. 3) where the *lower* curves are the LIS ratio. The modulation on these plots has been done using the force field approximation. For the B/C ratio (Fig. 3) in the DC model the result of modulation in the drift model is also shown though the difference (force field approximation vs. drift model) is small.

The "tertiary" antiprotons (inelastically scattered secondaries), significant at the lowest energies, are important in interstellar space but make no difference when compared with measurements in the heliosphere (Fig. 7).

The DR model reproduces the sharp peak in secondary to primary nuclei ratios (Strong & Moskalenko 1998, 2001). However, this model produces a bump in proton and He spectra at ~ 2 GeV nucleon^{-1} that is not observed.[7] This bump can be removed by choosing an injection spectrum that is flatter at low energies (see, e.g., Jones et al. 2001). There are however some problems with secondaries such as positrons and antiprotons which are difficult to manage. A similar bump appears in the positron spectrum at ~ 1 GeV, and the model underproduces antiprotons at 2 GeV by more than 30%.

[7] A similar bump is produced also in the electron spectrum at 1 GeV.

TABLE 4

PROPAGATION PARAMETER SETS

		DIFFUSION COEFFICIENT[b]		REACCELERATION/CONVECTION[c]	
MODEL	INJECTION INDEX, γ[a]	D_0 ($\mathrm{cm^2\ s^{-1}}$)	Index, δ	$v_A/w^{1/2}$ ($\mathrm{km\ s^{-1}}$)	dV/dz ($\mathrm{km\ s^{-1}\ kpc^{-1}}$)
Diffusive reacceleration (DR)	2.43	6.10×10^{28}	0.33	30	...
Diffusive reacceleration with break (DRB)	1.93/2.43[d]	6.10×10^{28}	0.33	30	...
Minimal reacceleration plus convection (MRC)	2.43	4.30×10^{28}	0.33	17	10
Plain diffusion (PD)	2.16	3.10×10^{28}	0.60	...	...
Diffusion plus convection (DC)	2.46/2.16[e]	2.50×10^{28}	0/0.60[a]	...	10

NOTE.—Adopted halo size $z_h = 4$ kpc.

[a] For a power law in rigidity, $\propto \rho^{-\gamma}$.

[b] $\rho_0 = 4$ GV, index δ is shown below/above ρ_0.

[c] v_A is the Alfvén speed, and w is defined as the ratio of MHD wave energy density to magnetic field energy density.

[d] Index below/above rigidity 10 GV.

[e] Index below/above rigidity 20 GV.

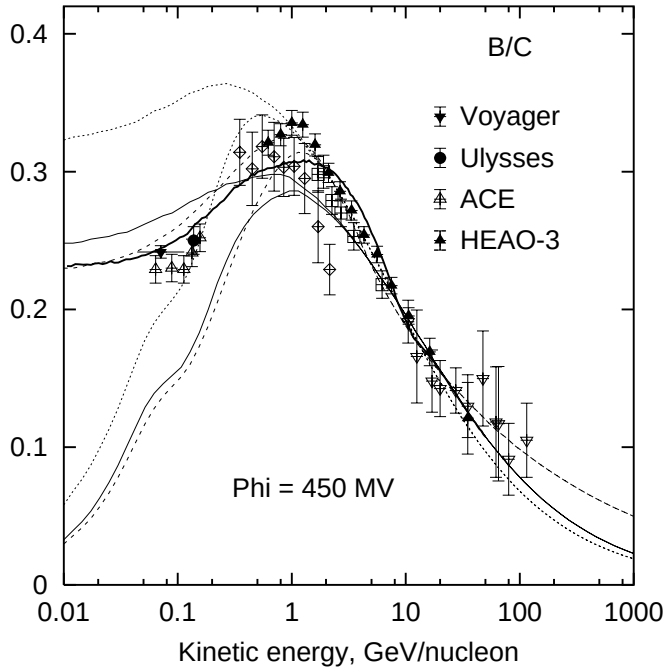

FIG. 3.—B/C ratio as calculated in DC, DR, and PD models for $z_h = 4$ kpc. *Lower curves:* interstellar; *upper curves:* modulated ($\Phi = 450$ MV). The line coding is solid lines for the DC model, dashed lines for the DR model, and dotted lines for the PD model. The thick solid line (DC model) corresponds to the drift model calculations of heliospheric modulation for $A > 0$ and tilt angle 5°. Data below 200 MeV nucleon^{-1}: *ACE* (Davis et al. 2000), *Ulysses* (DuVernois, Simpson, & Thayer 1996), *Voyager* (Lukasiak, McDonald, & Webber 1999); high-energy data: *HEAO 3* (Engelmann et al. 1990); for other references see Stephens & Streitmatter (1998).

In order to fit the proton/He spectra in a diffusive reacceleration model, we need to introduce a break in the injection spectrum, with a smaller index below 10 GV (model DRB, *not* shown in the plot for clarity). This break in the injection spectrum of primaries results in smaller bump in the secondary positron spectrum (Fig. 6, *dot-dashed line*), though the predicted spectrum still shows a significant excess of a factor at least 2 over the measurements. However, it produces no effect on secondary antiprotons because of their higher production threshold energy. Taken together these cases provide evidence against "strong" reacceleration[8] in the interstellar medium (ISM).

Another model combining reduced reacceleration and convection (MRC) also produces too few antiprotons.

Using the PD model we can get good agreement with B/C above a few GeV nucleon^{-1}, with nucleon spectra and positrons, but this model overproduces antiprotons at 2 GeV by $\sim$20% and contradicts the secondary/primary nuclei ratio (B/C) below 1 GeV nucleon^{-1}.

The DC model is our "best-fitting model." It reproduces all the particle data "on average," although it has still some problem with reproduction of the sharp peak in the B/C ratio. In this model a flattening of the diffusion coefficient ($\delta = 0$) below 4 GV is required to match the B/C ratio at low energies. A possible physical origin for the behavior of the diffusion coefficient is discussed in § 5.3.

To better match primaries (p, He) in the DC model, we introduced a steeper injection spectrum below 20 GV to compensate the break in the diffusion coefficient, which tends to flatten the spectrum at low energies. Such a steepening in the injection spectrum, however, has almost no effect on secondaries ($\bar{p}$, e^+). The existence of a sharp upturn below a few GeV nucleon^{-1} is in fact predicted from SNR shock acceleration theory (Ellison et al. 2001); this is a transition region between thermal and nonthermal particle populations in the shock. Our model does not require a

[8] We define that the reacceleration is "strong" if the model is able to match the B/C ratio without invoking other mechanisms such as convection and/or breaks in the diffusion coefficient.

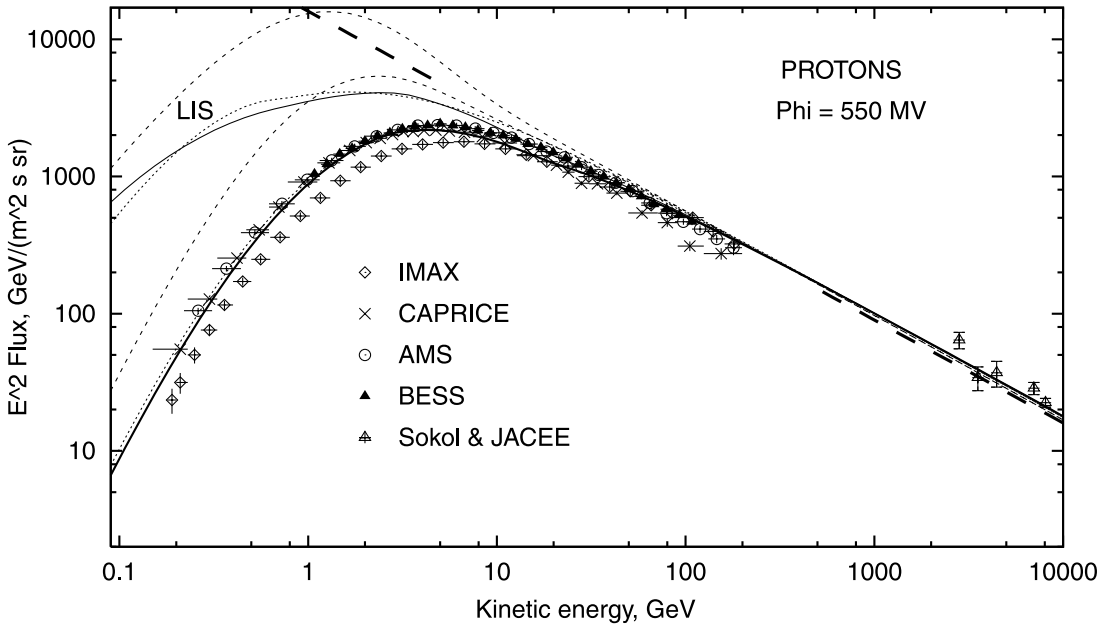

FIG. 4.—Calculated proton interstellar spectrum (LIS) and modulated spectrum (force field, $\Phi = 550$ MV). The lines are coded as in Fig. 3. Thick dashed line shows our composite spectrum as derived from measurements $1.60 \times 10^4 E_{\rm kin}^{-2.75}$ m^{-2} s^{-1} sr^{-1} GeV^{-1} (not shown between 5 and 500 GeV for clarity). Data: IMAX (Menn et al. 2000), CAPRICE (Boezio et al. 1999), AMS (Alcaraz et al. 2000a), BESS (Sanuki et al. 2000), Sokol (Ivanenko et al. 1993), and JACEE (Asakimori et al. 1998).

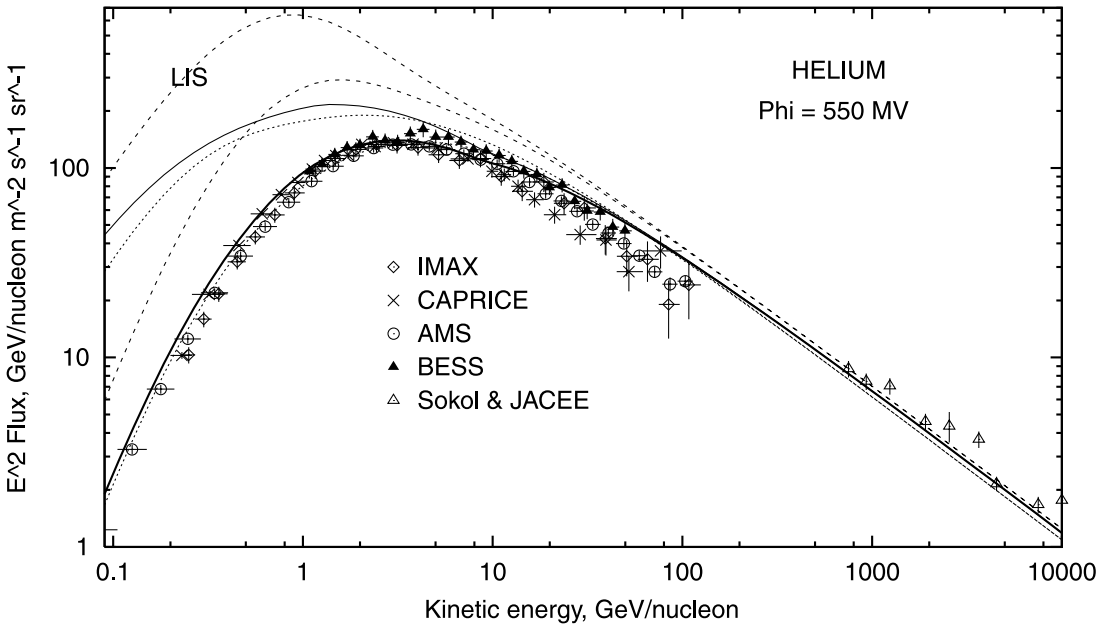

FIG. 5.—Calculated He interstellar spectrum (LIS) and modulated spectrum (force field, $\Phi = 550$ MV). The lines are coded as in Fig. 3. Data: IMAX (Menn et al. 2000), CAPRICE (Boezio et al. 1999), AMS (Alcaraz et al. 2000b), BESS (Sanuki et al. 2000), Sokol (Ivanenko et al. 1993), and JACEE (Asakimori et al. 1998).

large break (0.3 in index is enough; see Table 4). More discussion is given in §§ 5.3 and 7.

The drift model has been used for heliospheric modulation of all spectra obtained in the DC model (p, He, B/C, e^+, $\bar{p}$). The same modulation parameter set has been applied to all the species, and the agreement is good. The B/C ratio (Fig. 3) is virtually insensitive to the modulation level, and it remains the same for a wide variety of tilt angles.

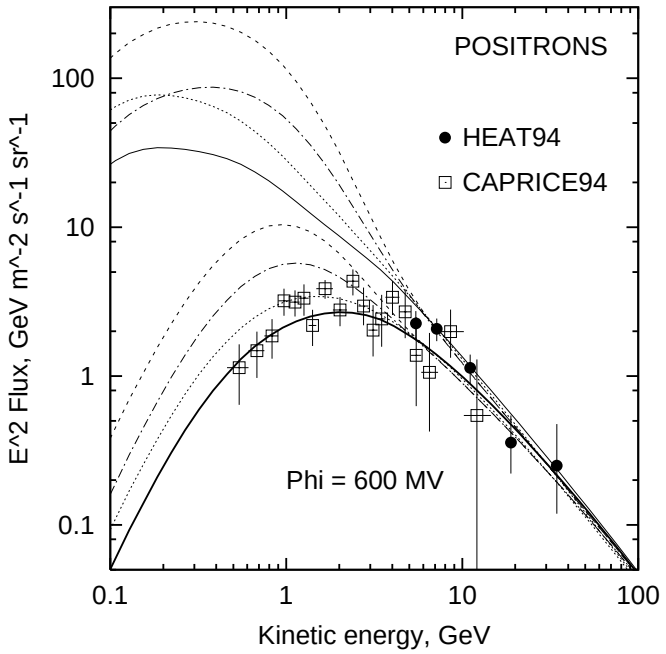

FIG. 6.—Calculated positron flux: upper curves for LIS, lower curves for modulated (force field, $\Phi = 600$ MV). The lines are coded as in Fig. 3. Positron flux as calculated in DRB model is shown by the dot-dashed line. Data: HEAT94 (Barwick et al. 1998), CAPRICE94 (Boezio et al. 2000).

5.3. *Discussion*

Our "best-fit" model (DC) with a constant diffusion coefficient below 4 GV suggests some change in the propagation mode. Propagation and scattering of the high-energy particles on magnetic turbulence are described by diffusion

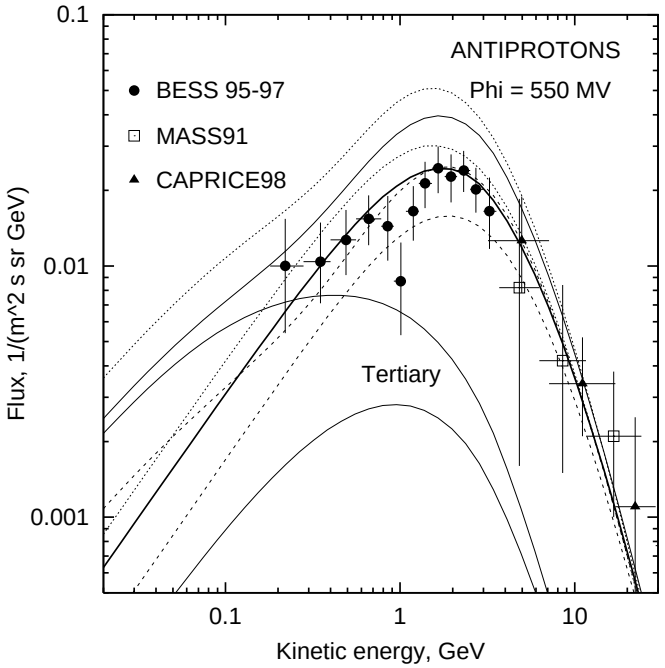

FIG. 7.—Calculated antiproton spectrum: upper curves for LIS; modulation was made with $\Phi = 550$ MV (force field, *lower curves*). The lines are coded as in Fig. 3. Data: BESS (Orito et al. 2000), MASS91 (Stochaj et al. 2001), CAPRICE98 (Boezio et al. 2001). The top curves are the total secondary $\bar{p}$ values. The two lowest curves marked "tertiary" show separately the LIS spectrum and modulated "tertiary" component in the DC model.

with the diffusion coefficient increasing with energy. The growth of the diffusion coefficient depends on the adopted spectrum of magnetic turbulence and is typically in the range 0.3–0.6. However, at low energies particles could propagate following the magnetic field lines rather than scatter on magnetic turbulence. This change in the propagation mode may affect the diffusion coefficient, making it less dependent on energy. Since the magnetic field lines are essentially tangled, such a process can still behave like diffusion (Berezinskii et al. 1990).

One more unknown variable is the CR spectrum in the distant regions of the Galaxy. The LIS nucleon spectrum is studied quite well by direct measurements at high energies where solar modulation effects are minimal. Meanwhile, the ambient CR proton spectrum on the large scale remains unknown. The most direct test is provided by diffuse γ-rays. However, there is the well-known puzzle of the GeV excess in the EGRET diffuse γ-ray spectrum (Hunter et al. 1997) which makes a direct interpretation in terms of protons problematic, and possibly IC emission from a hard electron spectrum is responsible (Strong et al. 2000); for this reason we do not consider γ-rays further here.

An interesting independent possibility to test the interstellar nucleon spectrum at different energies is provided by antiproton and positron data taken together. While the spectra of antiprotons and positrons at above $\sim$1 GeV allow conclusions on the nucleon spectrum above $\sim$10 GeV (Moskalenko et al. 1998), the positron spectrum below 1 GeV is sensitive to the nucleon spectrum below the antiproton production threshold $\sim$10 GeV. The problem here is that the propagation parameters are not known accurately enough, and this affects the predicted spectrum of positrons at low energies.

6. VARIATIONS OF PROTON AND ANTIPROTON SPECTRA OVER THE SOLAR CYCLES

We use the DC model to calculate the LIS spectra of protons and antiprotons and then use the drift model to determine their modulated spectra and ratio over the solar cycles with positive ($A > 0$) and negative ($A < 0$) polarity (Figs. 8–10). The variations shown depend on the tilt angle. When combined with Figure 2, this allows us to estimate the near-Earth spectra for arbitrary epochs in the past as well as make some predictions for the future. It may be also used to test the theory of heliospheric modulation.

The $\bar{p}/p$ ratio is supposed to be more accurately measured than the flux. Interestingly, the $\bar{p}/p$ ratio appears largely insensitive to the modulation level during the $A > 0$ cycle (Fig. 10, *left panel*). This agrees within the error bars with BESS $\bar{p}/p$ measurements made in 1993, 1995, 1997, 1998 (Maeno et al. 2001), and 1999 (Asaoka et al. 2001b) and thus allows us to constrain the proton spectrum at low energies, in the heliosphere above $\sim$0.1 GeV and the LIS spectrum above $\sim$0.7 GeV. In the new cycle ($A < 0$), on the contrary, this ratio is predicted to vary by over an order of magnitude (Fig. 10, *right panel*), which will allow us to validate the calculations of heliospheric modulation including charge sign effects. Our predictions for tilt angles 55°–65° (indicated by the arrow) agree well with the data from the BESS 2000 flight (Asaoka et al. 2001b). The HEAT 2000 data (Musser et al. 2001) were obtained during the Spring 2000 flight at around the solar maximum, but the solar modulation is weak at high energies. Shown also are two data points obtained at the moderate level of solar activity

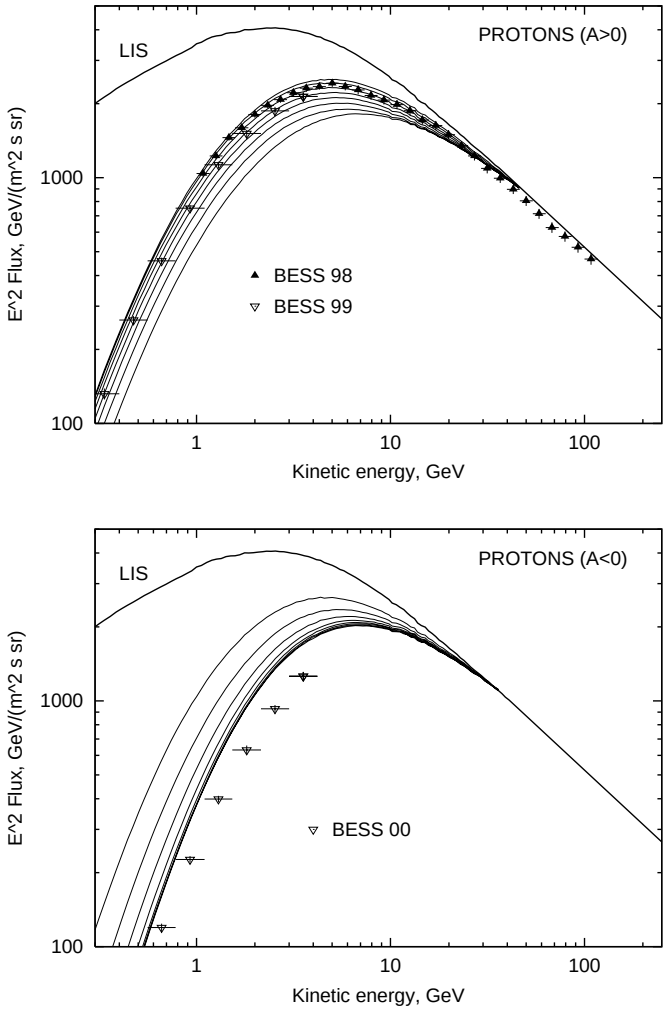

FIG. 8.—Calculated proton LIS and modulated spectra for the two magnetic polarity-dependent modulation epochs, $A > 0$ (*top*) and $A < 0$ (*bottom*). Tilt angle from top to bottom: 5°, 15°, 25°, 35°, 45°, 55°, 65°, 75°. The tilt angle corresponding to BESS 1998 data is $\sim$5°–15° ($A > 0$) depending on the coronal field model. For discussion of BESS 1999 and 2000 data see text. Data: BESS 1998 (Sanuki et al. 2000), BESS 1999, BESS 2000 (Asaoka et al. 2001b).

in 1984–1985 and 1986–1989 in the previous $A < 0$ cycle (Bogomolov et al. 1987, 1990; E. A. Bogomolov 2001, private communication).

The proton flux data obtained during BESS 1999 and 2000 flights (Asaoka et al. 2001b) agree qualitatively with variations over the solar cycle. However, BESS 1999 data show a flux which is somewhat larger while BESS 2000 data show the flux lower than predicted. Both measurements have been made during maximum solar activity and near the solar magnetic field reversal and may reflect the dynamic effects taking place in the heliosphere.

Now we use the predicted variations over the solar cycle to combine BESS data collected in 1995 and 1997 during the solar minimum with BESS data collected in 1998, when the solar activity was moderate (the tilt angle about 25°). The correction was calculated using the energy-dependent factor, $F(E)_{5/25} = \psi_5/\psi_{25}$, the ratio of modulated antiproton spectra with tilt angles 5° and 25°. The data of 1998 and their error bars have been multiplied by this factor. The spectrum obtained in such a way has been further combined with BESS data collected in 1995 and 1997.

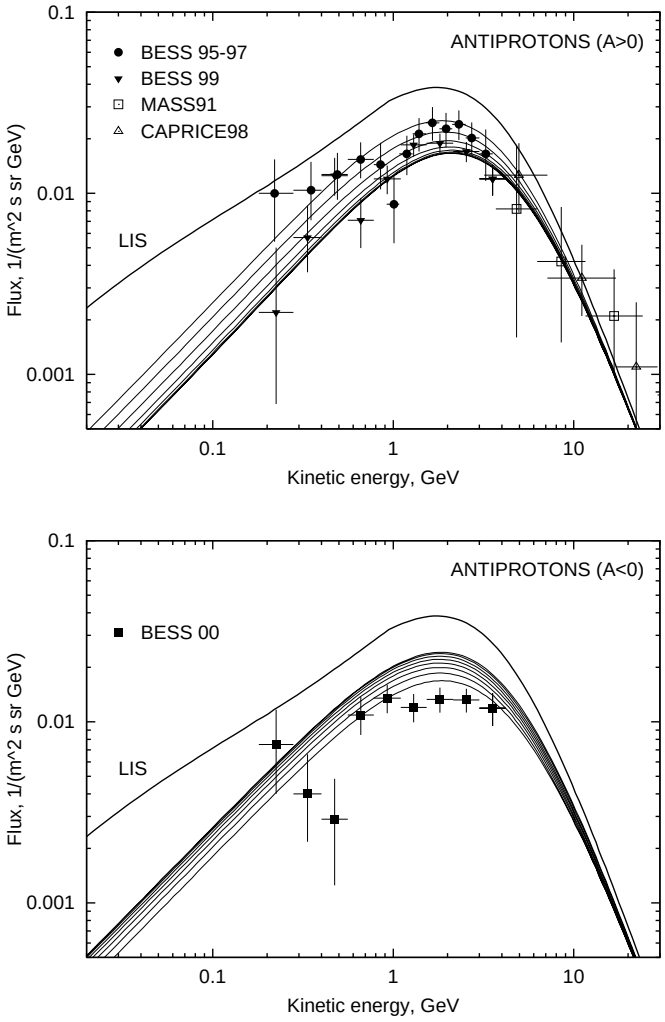

FIG. 9.—Calculated antiproton LIS and modulated spectra for the two magnetic polarity-dependent modulation epochs, $A > 0$ (*top*) and $A < 0$ (*bottom*). Tilt angle from top to bottom: 5°, 15°, 25°, 35°, 45°, 55°, 65°, 75°. The tilt angle corresponding to BESS data is ~5°–15° ($A > 0$) depending on the coronal field model. Data references as in Fig. 7, BESS 1999, BESS 2000 (Asaoka et al. 2001b).

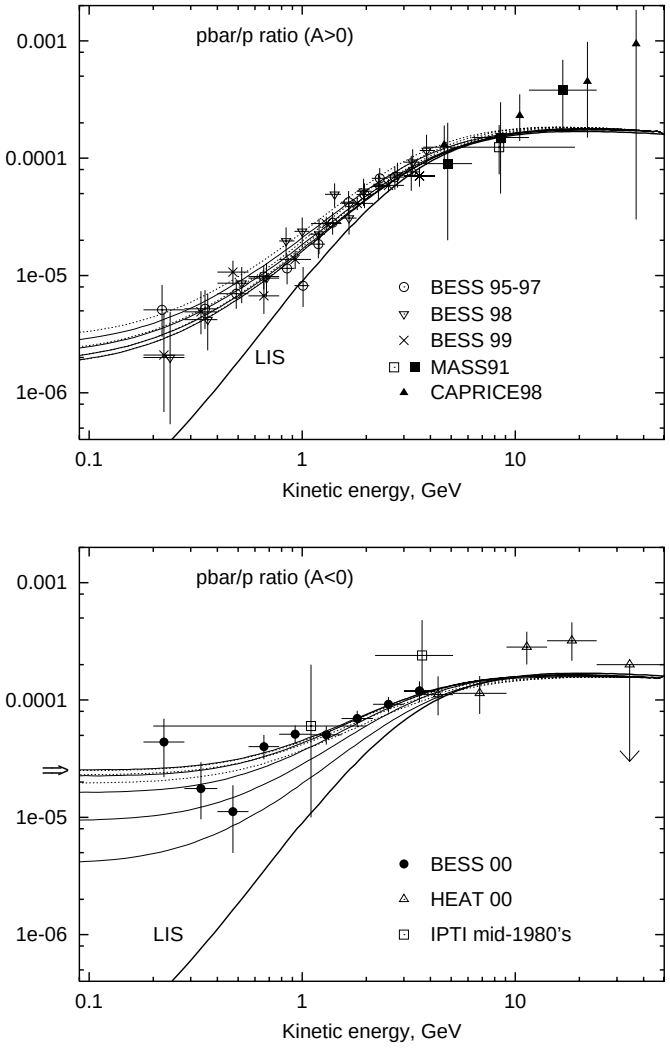

FIG. 10.—Calculated $\bar{p}/p$ ratio in the ISM (LIS) and modulated for the two magnetic polarity-dependent modulation epochs, $A > 0$ and $A < 0$. *Top:* Tilt angle from top to bottom (*solid lines*): 5°, 15°, 25°, 35°; from top to bottom (*dotted lines*): 75°, 65°, 55°, 45°. (Lines almost coincide for the tilt angles 35°, 45° and 25°, 55°, and very close for 15°, 65°.) Data: BESS (Orito et al. 2000; Maeno et al. 2001; Asaoka et al. 2001b), MASS91 (Hof et al. 1996; Stochaj et al. 2001), CAPRICE98 (Bergström et al. 2000). *Bottom:* Tilt angle from bottom to top (*solid lines*): 5°, 15°, 25°, 35°, 45°; from bottom to top (*dotted lines*): 75°, 65°, 55°. (Lines are very close for the tilt angles 35°, 65° and 45°, 55°.) The BESS 2000 data agree well with our predictions for the tilt angles 55°–65° (indicated by the arrow). Data: IPTI (Bogomolov et al. 1987, 1990), HEAT 2000 (Musser et al. 2001), BESS 2000 (Asaoka et al. 2001b).

The combined spectrum agrees very well with calculations for tilt angle 5° and $A > 0$ (Fig. 11). It is, however, not sensitive to the exact value of the tilt angle at the epoch of the BESS 1998 flight. It looks very similar for tilt angles 15° and 35°. The reason is that the error bars of the data collected in 1998 are large, so that their relative weight is small.

TABLE 5

SUMMARY OF MODEL PREDICTIONS

		PRIMARIES		SECONDARIES	
MODEL	B/C	Protons	He	Antiprotons	Positrons
DR[a]	Good	Low-energy bump/Good	Fair/Good	Too few	Low-energy bump
DRB	Good	Good	Good	Too few	Low-energy excess
MRC[a]	Fair	Low-energy bump/Good	Fair/Good	Too few	Low-energy bump
PD	Too large at low energy	Good	Good	Too many	Good
DC	Fair	Good	Good	Good	Good

[a] The reproduction of spectra of primaries can be improved by choice of the injection spectrum.

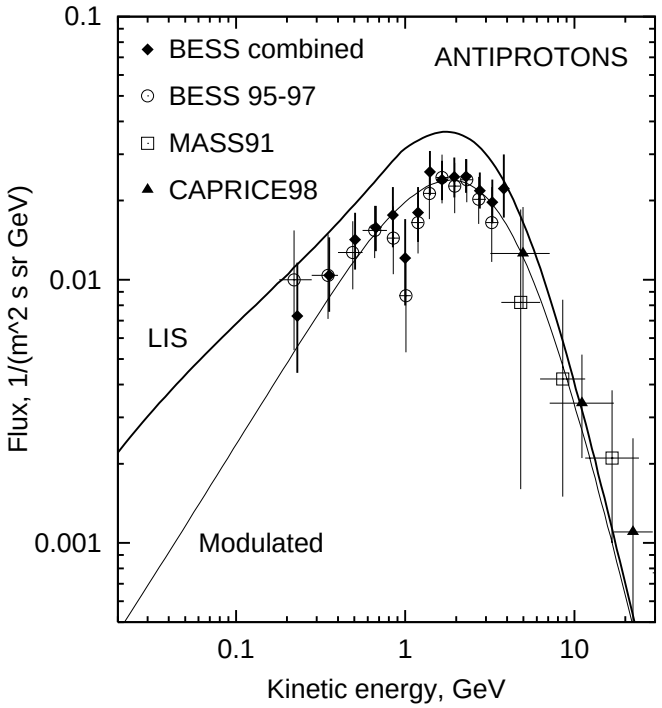

FIG. 11.—BESS 1995–1997 data and the data combined with "corrected" BESS 1998 measurements. Shown also are the calculated antiproton interstellar (LIS) and modulated spectrum for a tilt angle 5° ($A > 0$). Data references as in Fig. 7.

7. CONCLUSIONS

In this paper we have studied five basic propagation models. Table 5 summarizes the results of this study. First, we applied a propagation model with reacceleration. It reproduces nuclear secondary/primary ratios rather well but has some difficulties with reproduction of primary proton and He spectra and, more importantly, with secondary positrons and antiprotons. When the primary injection spectra are adjusted to fit the observed modulated p and He spectra, the secondary positron excess is reduced but still significant, while the antiproton deficit is unaffected. Another model with reduced reacceleration strength and convection also produces too few antiprotons. A plain diffusion model (no reacceleration, no convection) reproduces the high-energy part of nuclear secondary/primary ratios, protons, and positrons, but it has a problem with the low-energy part of nuclear secondary/primary ratios and overestimates the antiproton flux. A model with convection and flattening of the diffusion coefficient at low energies and a break in the injection spectrum is our "best-fit" model. It reproduces well all particle data "on average." The spectrum of diffuse γ-rays calculated for this model cannot explain the EGRET GeV excess (Hunter et al. 1997), but this could originate in other ways.

During the last decade there have been a number of space and balloon experiments with improved sensitivity and statistics. They impose stricter constraints on the CR propagation models. It has become clear that currently there is no *simple* model that is able to simultaneously reproduce all data related to CR origin and propagation. This conclusion is mainly the result of the increased precision of the CR experimental data, but also the improved reliability of the calculations of interstellar and heliospheric propagation.

What could be the origin of this failure (to find a simple model), apart from the propagation models? Concerning the accuracy of the experimental data, the spectra of protons and helium are measured almost simultaneously and quite precisely by BESS and AMS, and the agreement is impressive. They also agree with earlier experiments, such as LEAP, IMAX, and CAPRICE, within the error bars. The most accurate measurements of nuclei at low energies are made by *Voyager*, *Ulysses*, and the *Advanced Composition Explorer* (*ACE*), and the agreement is good. At higher energies the data obtained by *HEAO 3* are the most accurate and generally agree with earlier measurements. Electron flux measurements made by HEAT, CAPRICE, and at the Sanriku balloon facility all agree. Positron data, though with large error bars, are in agreement as well. The possibility that BESS antiproton data have systematic errors as large as 20% looks improbable. They have carried out calibrations which demonstrate that the error must be $\leq 5\%$ (Asaoka et al. 2001a). However, additional measurements are desirable.

Nuclear cross section errors are one of the main concerns. Fitting (matching) the measured B/C ratio is a standard procedure to derive the propagation parameters. The calculated ratio, in turn, depends on many cross sections, such as the total interaction and isotope production cross sections. The latter appear to have quite large uncertainties, typically about 20%, and sometimes they can even be wrong by an order of magnitude (see, e.g., Moskalenko et al. 2001a). This is reflected in the value of the diffusion coefficient, the Alfvén velocity (parameterizing reacceleration) and/or convection velocity, and thus influences the calculated spectra of CR species. Our cross section calculations make use of the fits to the cross sections p + C, N, O → Be, and B, which produce most of the Be and B. Other channels are calculated using the Webber et al. (1990) or Silberberg et al. (1998) cross section codes renormalized to data where they exist. We thus can rule out a possibility of large errors in the calculated B/C ratio.

Solar modulation for antiprotons is different from that of protons, the effect known as charge sign dependence. Over the last years *Ulysses* made its measurements at different heliolatitudes so we know more about the solar magnetic field configuration and the solar wind velocity distribution. On the other hand, the two *Voyager* satellites, the most distant spacecraft, provide us with measurements of particle fluxes made close to the heliospheric boundary. There is thus a small chance of a serious error, e.g., that the antiproton flux during the last solar minimum was modulated much more weakly than estimated.

The underproduction of antiprotons in the reacceleration model may be connected with a contribution of primary antiprotons, but this suggestion conflicts with other CR data. A strong primary antiproton signal would be accompanied by the positron signal and an excess in γ-rays (EGRET GeV excess?). However, the positron flux calculated in the DR model already shows an excess rather than a deficit. Besides, only a few SUSY dark matter candidates are able to produce a signal large enough to be detected, and even in this case primary antiprotons contribute mostly to low energies (see discussions in Bottino et al. 1998; Bergström, Edsjö, & Ullio 1999).

Considering reacceleration models, there is the possibility that the injection spectra of protons and nuclei might be different. For instance, spectra of nuclei $Z > 2$ are well

reproduced by a reacceleration model with a power-law (in rigidity) injection spectrum, while protons, helium, and electrons require some spectral flattening at low energies to avoid developing a bump in the spectrum. This is in agreement with conclusions made by other authors (Jones et al. 2001). The difficulty is to get the right positron and antiproton fluxes in the reacceleration model. On the other hand, non-reacceleration models require some spectral steepening at low energies (compensation for flattening of the diffusion coefficient) to get good agreement with the spectra of primaries. Such steepening may be a consequence of SNR shock acceleration (Ellison et al. 2001).

If we assume that the problem is in propagation models, we have shown that it *is* possible to construct a model (DC) that fits all these data, by postulating a significant flattening of the diffusion coefficient below 4 GV together with convection (and possibly with some reacceleration) and a break in the injection spectrum. The break in the diffusion coefficient is reminiscent of the standard procedure in "leaky box" models where the escape time is set to a constant below a few GeV. This has always appeared a completely ad hoc device without physical justification, but the present analysis suggests that it may be forced on us by the data. Therefore, possibilities for its physical origin should be studied.

Where do we go from here? New measurements of CR species that cover the range 0.5–1000 GeV nucleon^{-1} are necessary to distinguish between reacceleration and non-reacceleration models. The new experiment *PAMELA* scheduled for launch in 2002 should improve accuracy of positron (0.1–200 GeV) and electron (0.1–300 GeV) measurements while allowing for simultaneous measurements of $\bar{p}$ and nuclei from H to C in the energy range 0.1–200 GeV nucleon^{-1} (*PAMELA* Collaboration 1999). The puzzling excess in the diffuse γ-rays above 1 GeV in EGRET data should be confirmed. Here we await the launch of *GLAST* with 30 times better sensitivity. Its improved angular resolution will be helpful in removing the unresolved source component contribution to the diffuse flux. A possibility that the nucleon spectrum in the Galaxy is harder or softer than we measure locally should be explored by making more accurate measurements of antiproton fluxes at high energies (Moskalenko et al. 1998). This may help to produce more antiprotons in the DR model and simultaneously explain the GeV excess in γ-rays. The interpretation of B/C and other secondary/primary ratios depends on the assumption that all the secondaries are produced during propagation; if instead some secondary production occurs in the sources, the range of possible models widens. Whether such effects could provide an alternative explanation of the observed effects should be the subject of future study. The effect of the local distribution of interstellar matter is worth investigating, and we are going to do this in the future by developing and incorporating in our code a three-dimensional model of the gas distribution in the Galaxy. The effect should however be only important for radioactive and K-capture isotopes and electrons/positrons, i.e., for those particles whose half-life is less or

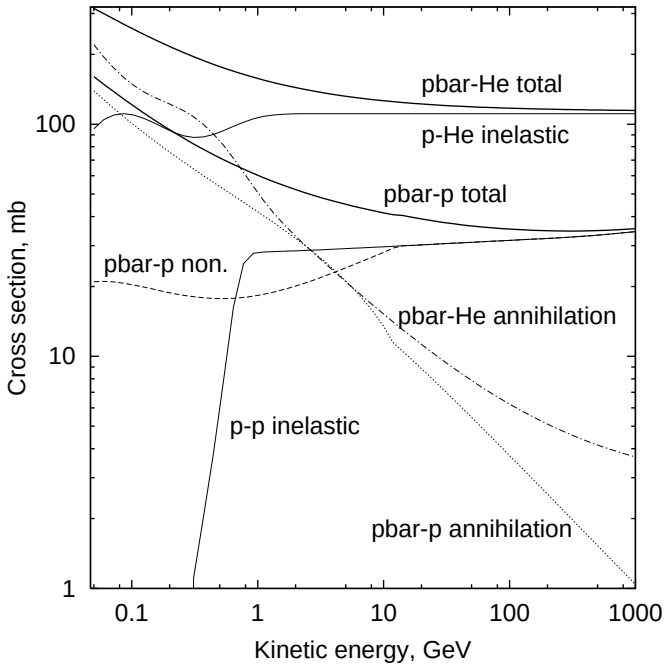

FIG. 12.—Proton and antiproton cross sections

comparable to the CR lifetime in the Galaxy or whose large energy losses confine them to a short distance from the source. On the other hand, for protons, with their 30 mbarn total cross section and negligible energy losses, only the large-scale gas distribution is important. The same is true for antiprotons, as their total interaction cross section at 1 GeV is only about 2 times larger and approaches the proton cross section at higher energies (Fig. 12). A thorough and systematic measurement of the nuclear cross sections over a wide energy range is extremely important. Accurate measurements of the cross sections would allow more information to be extracted from the now rather precise CR measurements. New measurements of the antiproton and charged and neutral pion production cross sections are desirable. The widely used parameterization of antiproton production and interaction cross sections by Tan & Ng (1983a, 1983b) is 20 yr old. Parameterization of pion production is even older. Given the new experimental techniques now available, such measurements should be straightforward. At the same time, the sensitivity of the whole analysis to the modulation models has to be investigated further.

The authors are grateful to Frank Jones and Vladimir Ptuskin for fruitful discussions, to Don Ellison for discussions and a copy of his manuscript prior to publication, to S. A. Stephens and R. A. Streitmatter for providing the database of CR measurements, and to Ulrich Langner for his interest and assistance in producing modulation runs for Figures 8–10. I. V. M. acknowledges support from NAS/NRC Research Associateship Program.

APPENDIX A

THE INTERSTELLAR GAS DENSITY DISTRIBUTION IN THE CYLINDRICALLY SYMMETRICAL MODEL

The H_2 number density in mol cm^{-3} is calculated from

$$n_{H_2}(R, z) = 3.24 \times 10^{-22} X \epsilon_0(R) e^{-\ln 2(z-z_0)^2/z_h^2}, \tag{A1}$$

where $\epsilon_0(R)$ (K km s^{-1} kpc^{-1}) is the CO volume emissivity, $z_0(R)$ and $z_h(R)$ are the height scale and width defined by a table (Bronfman et al. 1988), and $X \equiv n_{H_2}/\epsilon_{CO} = 1.9 \times 10^{20}$ mol cm^{-2}/(K km s^{-1}) is the conversion factor (Strong & Mattox 1996).

The H I (atom cm^{-3}) relative distribution is taken from Gordon & Burton (1976) but renormalized to agree with Dickey & Lockman (1990), since they give their best model for the z-distribution in the range $R = 4$–8 kpc and state that the total integral perpendicular to the plane is 6.2×10^{20} cm^{-2}:

$$n_{H\ I}(R, z) = \frac{1}{n_{GB}} Y(R) \begin{cases} \sum\limits_{i=1,2} A_i e^{-\ln 2(z^2/z_i^2)} + A_3 e^{-|z|/z_3} & R \le 8 \text{ kpc}, \\ \text{interpolated} & 8 < R < 10 \text{ kpc}, \\ n_{DL} \exp(-z^2 e^{-0.22R}/z_4^2) & R \ge 10 \text{ kpc}. \end{cases} \tag{A2}$$

Here $Y(R)$ is the distribution from Gordon & Burton (1976) ($R < 16$ kpc), and $n_{GB} = 0.33$ cm^{-3} and $n_{DL} = 0.57$ cm^{-3} are the disk densities in the range $4 < R < 8$ kpc in models by Gordon & Burton (1976) and Dickey & Lockman (1990), respectively. The z-dependence is calculated using the approximation by Dickey & Lockman (1990) for $R < 8$ kpc, using the approximation by Cox, Krügel, & Mezger (1986) for $R > 10$ kpc, and interpolated in between, and the parameter values are $A_1 = 0.395$, $A_2 = 0.107$, $A_3 = 0.064$, $z_1 = 0.106$, $z_2 = 0.265$, $z_3 = 0.403$, $z_4 = 0.0523$. For $R > 16$ kpc an exponential tail is assumed with scale length 3 kpc.

The ionized component H II (atom cm^{-3}) is calculated using a cylindrically symmetrical model (Cordes et al. 1991):

$$n_{H\ II}(R, z) = \sum_{i=1,2} n_i \exp\left[-\frac{|z|}{h_i} - \frac{(R - R_i)^2}{a_i^2}\right], \tag{A3}$$

where $n_1 = 0.025$, $n_2 = 0.200$, $h_1 = 1$ kpc, $h_2 = 0.15$ kpc, $R_1 = 0$, $R_2 = 4$ kpc, $a_1 = 20$ kpc, $a_2 = 2$ kpc.

APPENDIX B

PROTON AND ANTIPROTON CROSS SECTIONS

The energy and momentum units are GeV and GeV c^{-1}, respectively. All cross sections given are in mbarn and plotted in Figure 12 (except for the production cross section). An asterisk marks the center-of-mass (CMS) system variables.

The inclusive antiproton production cross section (mbarn GeV^{-2} c^3) in p-p reaction is given by (Tan & Ng 1983b)

$$\begin{aligned} E_{\bar{p}} \frac{d^3\sigma}{dp_{\bar{p}}^3} &= \delta(x_t) f(x_r) \exp[-A(x_r) p_t + B(x_r) p_t^2], \\ f &= 1.05 \times 10^{-4} \exp(-10.1 x_r) \theta(0.5 - x_r) + 3.15(1 - x_r)^{7.9}, \\ A &= 0.465 \exp(-0.037 x_r) + 2.31 \exp(0.014 x_r), \\ B &= 0.0302 \exp[-3.19(x_r + 0.399)](x_r + 0.399)^{8.39}, \\ x_r &= \frac{E_{\bar{p}}^*}{E_{\bar{p}}^{*\ \max}}, \end{aligned} \tag{B1}$$

where $\theta(x)$ is the Heaviside step function [$\theta(x > 0) = 1$, otherwise equal to 0], p_t is the transverse momentum of the antiproton, $E_{\bar{p}}^*$ is the total CMS energy of the antiproton, $E_{\bar{p}}^{*\ \max}$ is the maximal value of $E_{\bar{p}}^*$ for the given inclusive reaction, and $\delta(x_t)$ is the low-energy correction, $\delta = 1$ at $s^{1/2} > 10$ GeV. At $s^{1/2} \le 10$ GeV it is given by

$$\begin{aligned} \delta^{-1} &= 1 - \exp(-\exp[c(x_t) Q - d(x_t)]\{1 - \exp[-a(x_t) Q^{b(x_t)}]\}), \\ a &= 0.306 \exp(-0.12 x_t), \\ b &= 0.0552 \exp(2.72 x_t), \\ c &= 0.758 - 0.68 x_t + 1.54 x_t^2, \\ d &= 0.594 \exp(2.87 x_t), \\ Q &= \sqrt{s} - 4M_p, \\ x_t &= \frac{T_{\bar{p}}^*}{T_{\bar{p}}^{*\ \max}}, \end{aligned} \tag{B2}$$

where $s = 2M_p(E_{\bar{p}} + M_p) = \mathrm{inv}$ is the square of the total CMS energy of colliding particles, M_p is the proton rest mass, $T^*_{\bar{p}}$ is the kinetic CMS energy of antiproton, and $T^{*\ \max}_{\bar{p}}$ is the maximal value of $T^*_{\bar{p}}$ for the given inclusive reaction.

The proton-proton inelastic cross section is given by (Tan & Ng 1983a)

$$\sigma_{pp}^{\mathrm{inel}} = 32.2[1 + 0.0273U + 0.01U^2\theta(U)]\begin{cases} 0 & T_p < 0.3\ , \\ (1 + 2.62 \times 10^{-3}T_p^{-C})^{-1} & 0.3 \le T_p < 3\ , \\ 1 & T_p \ge 3\ , \end{cases}$$

$$U = \ln\left(\frac{E_p}{200}\right),$$

$$C = 17.9 + 13.8 \ln T_p + 4.41 \ln^2 T_p\ , \tag{B3}$$

where $\theta(U)$ is the Heaviside step function and E_p and T_p are the total and kinetic energy of proton, respectively.

The nucleus-proton inelastic cross section is given by (Letaw et al. 1983)

$$\sigma_{pA}^{\mathrm{inel}} = 45A^{0.7}\delta(T_p)[1 + 0.016 \sin (5.3 - 2.63 \ln A)]\begin{cases} 1 - 0.62e^{-T_p/0.2} \sin\left[\dfrac{10.9}{(10^3T_p)^{0.28}}\right] & T_p \le 3\ , \\ 1 & T_p > 3\ , \end{cases}$$

$$\delta = \begin{cases} 1 + 0.75 \exp\left(-\dfrac{T_p}{0.075}\right) & \text{for beryllium}\ , \\ 1 & \text{otherwise}\ , \end{cases} \tag{B4}$$

where A is the atomic number. In the case of p-He inelastic cross section equation (B5) is known to be not very accurate, while the p-^{4}He cross section is the most important after the p-p cross section. We thus made our own fit to the data in the range 0.02–50 GeV:

$$\sigma_{p\mathrm{He}}^{\mathrm{inel}} = 111(1 - \exp\,[-3.84(T_p - 0.1)]\{1 - \sin\,[9.72\log^{0.319}(10^3T_p) - 4.14]\})\ , \tag{B5}$$

where $T_p > 0.01$ GeV.

The antiproton-proton annihilation cross section at low energies is taken from Tan & Ng (1983a). At high energies it is calculated as the difference between the total $\bar{p}$-p and p-p cross sections which are parameterized using Regge theory (Groom et al. 2000):

$$\sigma_{\bar{p}p}^{a} = \begin{cases} 661(1 + 0.0115T_{\bar{p}}^{-0.774} - 0.948T_{\bar{p}}^{0.0151}) & T_{\bar{p}} \le 10\ , \\ 2 \times 35.43s^{-0.56} & T_{\bar{p}} > 10\ , \end{cases} \tag{B6}$$

where s is the square of the total CMS energy of colliding particles as defined in equation (B2). Annihilation is of minor importance at high energies.

The total *inelastic* antiproton-proton cross section is given by (Tan & Ng 1983a)

$$\sigma_{\bar{p}p}^{\mathrm{tot}} = \begin{cases} 24.7(1 + 0.584T_{\bar{p}}^{-0.115} + 0.856T_{\bar{p}}^{-0.566}) & T_{\bar{p}} \le 14\ , \\ \sigma_{pp}^{\mathrm{inel}} + \sigma_{\bar{p}p}^{a} & T_{\bar{p}} > 14\ . \end{cases} \tag{B7}$$

At very low energies, below $\sim$0.01 GeV, we put $\sigma_{\bar{p}p}^{a} = \sigma_{\bar{p}p}^{\mathrm{tot}}$.

The nonannihilation inelastic $\bar{p}$-p cross section is calculated as $\sigma_{\bar{p}p}^{\mathrm{non}} = \sigma_{\bar{p}p}^{\mathrm{tot}} - \sigma_{\bar{p}p}^{a}$. The antiproton-nucleus nonannihilation inelastic cross section is taken equal to proton-nucleus inelastic cross section, $\sigma_{\bar{p}A}^{\mathrm{non}} = \sigma_{pA}^{\mathrm{inel}}$.

The parameterization of the $\bar{p}$ total inelastic cross section on an arbitrary nuclear target has been obtained in Moiseev & Ormes (1997) using a parameterization by Kuzichev, Lepikhin, & Smirnitsky (1994) and has been tested against the data available on $\bar{p}$ cross sections on C, Al, and Cu targets:

$$\sigma_{\bar{p}A}^{\mathrm{tot}} = A^{2/3}[48.2 + 19T_{\bar{p}}^{-0.55} + (0.1 - 0.18T_{\bar{p}}^{-1.2})Z + 0.0012T_{\bar{p}}^{-1.5}Z^2]\ , \tag{B8}$$

where Z is the nucleus charge. The second term in square brackets has been modified from its original form $19(T_{\bar{p}} - 0.02)^{-0.55}$ to better match the slope below $\sim$100 MeV. This modification does not affect agreement with data at higher energies. Another modification, in the case of ^{4}He, is to use $A = 3.3$ to scale the value down slightly to be consistent with cross section data at both low and high energies (Allaby et al. 1971; Balestra et al. 1985).

The $\bar{p}$-A annihilation cross section is calculated from $\sigma_{\bar{p}A}^{a} = \sigma_{\bar{p}A}^{\mathrm{tot}} - \sigma_{\bar{p}A}^{\mathrm{non}}$, where $\sigma_{\bar{p}A}^{\mathrm{non}} = \sigma_{pA}^{\mathrm{inel}}$. This is quite accurate provided that the He abundance is about 10% that of H.

REFERENCES

Ahlen, S. P., et al. 1988, Phys. Rev. Lett., 61, 145
Alcaraz, J., et al. 2000a, Phys. Lett. B, 490, 27
———. 2000b, Phys. Lett. B, 494, 193
Allaby, J. C., et al. 1971, Soviet J. Nucl. Phys., 13, 295
Asakimori, K., et al. 1998, ApJ, 502, 278
Asaoka, Y., et al. 2001a, Nucl. Instrum. Methods Phys. Res. A, submitted (physics/0105003)
Asaoka, Y., et al. 2001b, Phys. Rev. Lett., submitted (astro-ph/0109007)
Ashman, K. M. 1992, PASP, 104, 1109
Badhwar, G. D., & O'Neill, P. M. 1996, Adv. Space Res., 17, 7
Balestra, F., et al. 1985, Phys. Lett. B, 165, 265
Barwick, S. W., et al. 1998, ApJ, 498, 779
Basini, G., et al. 1999, Proc. 26th Int. Cosmic-Ray Conf. (Salt Lake City), 3, 77

Belotti, R., et al. 1999, Phys. Rev. D, 60, 052002
Berezinskii, V. S., Bulanov, S. V., Dogiel, V. A., Ginzburg, V. L., & Ptuskin, V. S. 1990, Astrophysics of Cosmic Rays (Amsterdam: North Holland)
Bergström, D., et al. 2000, ApJ, 534, L177
Bergström, L., Edsjö, J., & Ullio, P. 1999, ApJ, 526, 215
Bieber, J. W., Burger, R. A., Engel, R., Gaisser, T. K., Roesler, S., & Stanev, T. 1999, Phys. Rev. Lett., 83, 674
Boezio, M., et al. 1999, ApJ, 518, 457
———. 2000, ApJ, 532, 653
———. 2001, ApJ, 561, 787
Bogomolov, E. A., et al. 1987, Proc. 20th Int. Cosmic-Ray Conf. (Moscow), 2, 72
———. 1990, Proc. 21st Int. Cosmic-Ray Conf. (Adelaide), 3, 288
Bogomolov, E. A., Lubyanaya, N. D., Romanov, V. A., Stepanov, S. V., & Shulakova, M. S. 1979, Proc. 16th Int. Cosmic-Ray Conf. (Kyoto), 1, 330
Bottino, A., Donato, F., Fornengo, N., & Salati, P. 1998, Phys. Rev. D, 58, 123503
Bronfman, L., Cohen, R. S., Alvarez, H., May, J., & Thaddeus, P. 1988, ApJ, 324, 248
Brückner, W., et al. 1986, Phys. Lett. B, 166, 113
Buffington, A., Schindler, S. M., & Pennypacker, C. R. 1981, ApJ, 248, 1179
Burger, R. A., & Potgieter, M. S. 1999, Proc. 26th Int. Cosmic-Ray Conf. (Salt Lake City), 7, 13
Burger, R. A., Potgieter, M. S., & Heber, B. 2000, J. Geophys. Res., 105, 27447
Carr, B. J. 1985, in Observational and Theoretical Aspects of Relativistic Astrophysics and Cosmology, ed. J. L. Sanz & L. J. Goicoechea (Singapore: World Scientific), 1
Chardonnet, P., Mignola, G., Salati, P., & Taillet, R. 1996, Phys. Lett. B, 384, 161
Cordes, J. M., Weisberg, J. M., Frail, D. A., Spangler, S. R., & Ryan, M. 1991, Nature, 354, 121
Cox, P., Krügel, E., & Mezger, P. G. 1986, A&A, 155, 380
Davis, A. J., et al. 2000, in AIP Conf. Proc. 528, Acceleration and Transport of Energetic Particles Observed in the Heliosphere (ACE-2000), ed. R. A. Mewaldt et al. (New York: AIP), 421
Dickey, J. M., & Lockman, F. J. 1990, ARA&A, 28, 215
Donato, F., Maurin, D., Salati, P., Barrau, A., Boudoul, G., & Taillet, R. 2001, ApJ, 563, 172
DuVernois, M. A., Simpson, J. A., & Thayer, M. R. 1996, A&A, 316, 555
Eisenhandler, E., et al. 1976, Nucl. Phys. B, 113, 1
Ellis, J., et al. 1988, Phys. Lett. B, 214, 403
Ellison, D. C., Slane, P., & Gaensler, B. M. 2001, ApJ, 563, 191
Engelmann, J. J., et al. 1990, A&A, 233, 96
Ferrando, P., Webber, W. R., Goret, P., Kish, J. C., Schrier, D. A., Soutoul, A., & Testerd, O. 1988, Phys. Rev. C, 37, 1490
Ferrari, A., Ranft, J., Roesler, S., & Sala, P. R. 1996, Z. Phys. C, 71, 75
Gaisser, T. K., & Levy, E. H. 1974, Phys. Rev. D, 10, 1731
Gaisser, T. K., & Schaefer, R. K. 1992, ApJ, 394, 174
Giacalone, J., & Jokipii, J. R. 1999, ApJ, 520, 204
Giacalone, J., Jokipii, J. R., & Kóta, J. 1999, Proc. 26th Int. Cosmic-Ray Conf. (Salt Lake City), 7, 37
Gleeson, L. J., & Axford, W. I. 1968, ApJ, 154, 1011
Golden, R. L., Horan, S., Mauger, B. G., Badhwar, G. D., Lacy, J. L., Stephens, S. A., Daniel, R. R., & Zipse, J. E. 1979, Phys. Rev. Lett., 43, 1196
Gordon, M. A., & Burton, W. B. 1976, ApJ, 208, 346
Groom, D. E., et al. 2000, European Phys. J., C15, 1
Hattingh, M., & Burger, R. A. 1995, Adv. Space Res., 16, 213
Hawking, S. W. 1974, Nature, 248, 30
HEGRA Collaboration 2000, A&A, 359, 682
Hoeksema, J. T. 1992, in Solar Wind Seven, ed. E. Marsch & R. Schwenn (Oxford: Pergamon), 191
Hof, M., et al. 1996, ApJ, 467, L33
Hunter, S. D., et al. 1997, ApJ, 481, 205
Ivanenko, I. P., et al. 1993, Proc. 23rd Int. Cosmic-Ray Conf. (Calgary), 2, 17
Jokipii, J. R., & Kóta, J. 1989, Geophys. Res. Lett., 16, 1
Jones, F. C., Lukasiak, A., Ptuskin, V., & Webber, W. 2001, ApJ, 547, 264
Jungman, G., & Kamionkowski, M. 1994, Phys. Rev. D, 49, 2316
Jungman, G., Kamionkowski, M., & Griest, K. 1996, Phys. Rep., 267, 195
Kiraly, P., Szabelski, J., Wdowczyk, J., & Wolfendale, A. W. 1981, Nature, 293, 120
Kuzichev, V. F., Lepikhin, Yu. B., & Smirnitsky, V. A. 1994, Nucl. Phys. A, 576, 581
Labrador, A. W., & Mewaldt, R. A. 1997, ApJ, 480, 371
Letaw, J. R., Silberberg, R., & Tsao, C. H. 1983, ApJS, 51, 271
Lukasiak, A., McDonald, F. B., & Webber, W. R. 1999, Proc. 26th Int. Cosmic-Ray Conf. (Salt Lake City), 3, 41
Maeno, T., et al. 2001, Astropart. Phys., 16, 121
Maki, K., Mitsui, T., & Orito, S. 1996, Phys. Rev. Lett., 76, 3474
Menn, W., et al. 2000, ApJ, 533, 281
Mewaldt, R. A., & Liewer, P. C. 2001, in The Outer Heliosphere: The Next Frontiers, ed. H. J. Fahr et al., in press
Mitchell, J. W., et al. 1996, Phys. Rev. Lett., 76, 3057
Moiseev, A. A., & Ormes, J. F. 1997, Astropart. Phys., 6, 379
Moskalenko, I. V., Mashnik, S. G., & Strong, A. W. 2001a, Proc. 27th Int. Cosmic-Ray Conf. (Hamburg), 1836 (astro-ph/0106502)
Moskalenko, I. V., & Strong, A. W. 1998, ApJ, 493, 694
———. 2000, Ap&SS, 272, 247
Moskalenko, I. V., Strong, A. W., Ormes, J. F., Potgieter, M. S., & Langner, U. 2001b, Proc. 27th Int. Cosmic-Ray Conf. (Hamburg), 1868 (astro-ph/0106503)
Moskalenko, I. V., Strong, A. W., & Reimer, O. 1998, A&A, 338, L75
Musser, J., et al. 2001, Proc. 27th Int. Cosmic-Ray Conf. (Hamburg), 1684
Orito, S., et al. 2000, Phys. Rev. Lett., 84, 1078
PAMELA Collaboration 1999, Proc. 26th Int. Cosmic-Ray Conf. (Salt Lake City), 5, 96
Parker, E. N. 1965, Planet. Space Sci., 13, 9
Potgieter, M. S. 1997, Adv. Space Res., 19, 883
———. 2000, J. Geophys. Res., 105, 18,295
Press, W. H., et al. 1992, Numerical Recipes in FORTRAN (2d ed.; Cambridge: Cambridge Univ. Press)
Roesler, S., Engel, R., & Ranft, J. 1998, Phys. Rev. D, 57, 2889
Rudaz, S. & Stecker, F. W. 1988, ApJ, 325, 16
Ryan, M. J., Ormes, J. F., & Balasubrahmanyan, V. K. 1972, Phys. Rev. Lett., 28, 985 (erratum 28, 1497)
Salamon, M. H., et al. 1990, ApJ, 349, 78
Sanuki, T., et al. 2000, ApJ, 545, 1135
Seo, E. S., Ormes, J. F., Streitmatter, R. E., Stochaj, S. J., Jones, W. V., Stephens, S. A., & Bowen, T. 1991, ApJ, 378, 763
Seo, E. S., & Ptuskin, V. S. 1994, ApJ, 431, 705
Silberberg, R., Tsao, C. H., & Barghouty, A. F. 1998, ApJ, 501, 911
Silk, J., & Srednicki, M. 1984, Phys. Rev. Lett., 53, 624
Simon, M., Molnar, A., & Roesler, S. 1998, ApJ, 499, 250
Stecker, F. W., & Tylka, A. J. 1989, ApJ, 336, L51
Stephens, S. A., & Streitmatter, R. A. 1998, ApJ, 505, 266
Stochaj, S. J., et al. 2001, ApJ, in press
Strong, A. W., & Mattox, J. R. 1996, A&A, 308, L21
Strong, A. W., & Moskalenko, I. V. 1998, ApJ, 509, 212
———. 1999, in Horizons in World Physics 230, Topics in Cosmic Ray Astrophysics, ed. M. A. DuVernois (New York: Nova Scientific), 81
———. 2001, Adv. Space Res., 27, 717
Strong, A. W., Moskalenko, I. V., & Reimer, O. 2000, ApJ, 537, 763 (erratum 541, 1109)
Szabelski, J., Wdowczyk, J., & Wolfendale, A. W. 1980, Nature, 285, 386
Tan, L. C., & Ng, L. K. 1983a, J. Phys. G, 9, 227
———. 1983b, J. Phys. G, 9, 1289
Trimble, V. 1987, ARA&A, 25, 425
Webber, W. R., Kish, J. C., & Schrier, D. A. 1990, Phys. Rev. C, 41, 566
Yamamoto, A., et al. 1993, Adv. Space Res., 14, 75
Yoshimura, K. 2001, Adv. Space Res., 27, 693
Yoshimura, K., et al. 1995, Phys. Rev. Lett., 75, 3792
Zank, G. P., Matthaeus, W. H., & Smith, C. W. 1996, J. Geophys. Res., 101, 17,093
Zhao, X., & Hoeksema, J. T. 1995, Adv. Space Res., 16, 181
Zirakashvili, V. N., Breitschwerdt, D., Ptuskin, V. S., & Völk, H. J. 1996, A&A, 311, 113